OPTICAL BREAKDOWN STRENGTH OF MATERIALS FOR HIGH-POWER LASERS

N. V. Morachevskii

A comprehensive investigation is reported of the physical processes that occur when laser radiation acts on optical materials (glass, fused quartz) during different stages of this action: the stage preceding the damage, bulk damage, and surface damage. A number of new experimental procedures is used. The kinetics of the development of the volume-damage zone is investigated in detail and the mechanism of this kinetics is established.

INTRODUCTION

When laser radiation interacts with transparent media, a number of effects are produced which are of great instructive and practical interest. These include all types of stimulated scattering, phenomena connected with nonlinear refraction, and others. In the study of these effects, the researchers came across the phenomenon of laser damage. This phenomenon consists in the fact that with increasing intensity and energy density of the laser radiation, the extinction coefficient increases sharply when certain critical (threshold) values of these quantities are exceeded. Depending on the experimental geometry and on the investigated material, this increase of the extinction coefficient has various outward manifestations: ejection (evaporation) of material from the surface, surface cracking, formation of internal faults as a result of melting, evaporation, or intense shattering of the materials. The net result is either a great decrease in the service life of a particular element of the optical system made of the corresponding material, or a situation wherein the intensity of the radiation passing through this element is limited, even in the first laser pulse, to the threshold value corresponding to the particular material.* Laser damage is frequently accompanied by rather intense optical and acoustic effects.

In most cases the faults due to laser damage are undesirable. These faults, first, limit the possibility of investigating nonlinear optical phenomena and, second, impose limitations on the output parameters of the lasers themselves, which use optical elements made of solid transparent dielectrics, such as laser rods, lenses, prisms, mirrors, nonlinear crystals, and others.

In connection with the rapid progress in laser technology and the development of new types of lasers, the applications of laser systems in various branches of sciences of technology become more extensive. From this point of view, laser damage is of economical interest to those who make use of these laser systems.

A number of assumptions have been made concerning the mechanisms that account for the laser damage. Two of the principal ones are: 1) absorption of the light by strongly absorbing inhomogeneities contained in the dielectric, followed by a thermal shock; 2) development of an electron avalanche in the dielectric, followed by absorption of the light by the free carriers, which leads to intense local overheating.

The historical development was such that those who studied laser damage produced by the action of a Q-switched laser, i.e., at nanosecond pulse durations, gave preference to the second mechanism. The apparent reason is the experimental fact that in this regime the threshold intensities reach values 10^9-10^{10} W/cm^2, which corresponds to electric field intensities $\sim 10^6$ V/cm. Such electric field intensities are of the same order as those at which electric breakdown takes place in a constant field.

*In this paper "damage threshold" is taken to mean that flux or energy density at which an irreversible change takes places in the optical characteristics of the material after the time of action of the radiation.

Translated from Trudy Ordena Lenina Fizicheskogo Instituta im. P. N. Lebedeva, Vol. 103, pp. 118-163, 1978.

0270-2010/80/0102-0089$07.50

Most workers investigating damage by radiation from a cw laser, i.e., in the range of millisecond pulse durations, adhered to the hypothesis that the laser radiation is absorbed by the strongly absorbing microscopic defects present in the dielectric. Contributing to this assumption were the lower threshold intensities compared with the Q-switched regime, $\sim 10^6$-10^8 W/cm^2, as well as some differences in the morphology of the damage picture.

Comparison of the experimental results obtained in these two regimes is hindered by certain accompanying effects observed near the laser-damage threshold. The most important of these accompanying effects are stimulated Mandel'shtam-Brillouin scattering and self-focusing. It is quite possible that under suitable experimental conditions these phenomena can influence in significant manner both the critical intensities and the kinetics of the laser-damage process.

All the foregoing pertains mainly to the so-called bulk damage. In addition to this damage there exists also surface damage. The terms "bulk" and "surface" damage are universally accepted. There is a difference between the surface and bulk damage thresholds. It should be noted that it is precisely surface damage which most frequently impedes the development of long-lived laser systems of high power. The damage of the surface of laser glasses usually takes place at lower intensity levels than in bulk damage. The damage to the reflecting coatings of the resonator mirrors should apparently also be classified as surface damage.

It can thus be concluded that a study of the physical processes on which laser damage is based is one of the urgent problems of modern quantum electronics.

According to present-day concepts, laser damage, from the point of view of its evolution, has two phases. The first phase, which precedes the loss of transparency, can be regarded as the analog of the subcritical growth of microcracks, which is the basis of mechanical damage, or of the latent induction period that precedes detonation in explosives. The second phase is the loss of transparency accompanied by the various effects mentioned above. There is no doubt that an investigation of each phase separately is of independent interest.

The present paper is devoted to an investigation of damage to optical materials used in high-power laser installations by radiation from a free-running neodymium laser. The first chapter contains a brief analysis of the principal mechanisms which are assumed at the present stage to be the basis of laser damage. The second chapter describes investigations, with the aid of a developed high-speed interferometry procedure, of optical effects that occur during the stage preceding the damage. The entire third chapter is devoted to comprehensive investigation of bulk damage: energy balance, kinetics of the damage zone, spectra, etc. The mechanism of development of the damage zone is discussed on the basis of the results. The kinetics of surface damage is the subject of the fourth chapter. The thermodynamic and gasdynamic parameters of the plasma flare produced in surface damage are measured. A mechanism of surface absorption during the stage of advanced evaporation is proposed.

CHAPTER I

MECHANISMS OF LASER DAMAGE OF TRANSPARENT DIELECTRICS

The study of laser damage of transparent dielectrics is the subject of a large number of scientific papers. Ready's book [1], in which one chapter is devoted to this problem, contains more than 100 literature references up to 1969. By now the number of papers on this problem has at least doubled. Systematization and a detailed analysis of these papers should apparently become the subject of a separate review article or even a book. This is not the task of the present paper. It is merely an attempt to cast light on the noted general tendencies in the views on the problem. The most important accompanying effects are also briefly considered.

As already noted in the Introduction, there are two principal laser-damage mechanisms: 1) damage by strongly absorbing inclusions, and 2) electron avalanche that develops as a result of impact ionization. These mechanisms will be discussed in the present chapter.

1. Interaction of Laser Radiation with Strongly Absorbing Inclusions

Relatively little work has been done on the theoretical analysis of the interaction of a high-power laser radiation with absorbing inclusions. The most detailed analysis was made within the framework of a linear approach.

In the first-order approximation, the included material is assumed to have extremely high thermal conductivity, so that the time of spreading of the heat over the volume of the

inclusion can be neglected. This approximation also gets around difficulties connected with the asymmetry of the irradiation geometry. The suprathermal-conduction approximation used for the inclusion is apparently valid if one of two inequalities are satisfied:

$$R_i \ll \sqrt{D_i \tau}, \tag{1}$$

where R_i is the radius of the inclusion; D_i, coefficient of thermal diffusivity of this material; and τ, characteristic heating time (e.g., the duration of the laser pulse), or else

$$R_i \ll k^{-1}, \tag{2}$$

where k is the absorption coefficient of the inclusion material (if the inclusion is sufficiently transparent). Which of these conditions is stronger depends on the values of D_i and k at the given duration τ. Thus, e.g., for noble metals condition (1) yields $R_i \ll 5 \cdot 10^{-4}$ cm at $\tau \simeq 10^{-6}$ sec. On the other hand, relation (2) yields $R_i \ll 10^{-6}$ cm, i.e., satisfies sufficiently well the condition (1).

Using this superthermally conducting inclusion approximation, an exact expression was obtained in [2] for the average inclusion temperature. This expression takes a simple form in two cases of practical importance. The first case is realized under the condition

$$R_i \gg \sqrt{D_g t}, \tag{3}$$

where D_g is the thermal-diffusivity coefficient of glass. Satisfaction of the second condition means that the thermal energy transferred from the inclusion to the glass can be neglected. In this case the expression for the average inclusion temperature takes the form

$$\bar{T} \simeq 3\varepsilon_\lambda J t / 4 c_{v_i} R_i, \tag{4}$$

where ε_λ is the absorptivity of the inclusion; J, laser-radiation flux density; and c_{vi}, specific heat per unit volume of the inclusion material. It is seen from (4) that the temperature is determined by the total energy absorbed by the instant of time t.

In the case when a condition inverse to (3) is satisfied, the expression for the temperature takes the form

$$\bar{T} \simeq \varepsilon_\lambda J R_i / 4 R_g, \tag{5}$$

where R_g is the thermal-conductivity coefficient of the glass, i.e., in this case the temperature is determined by the flux density J.

For typical values of D_g for glass, $3 \cdot 10^{-3}$ cm^2/sec, and pulse durations 10^{-6} sec, the inclusion size that determines the borderline between these regimes is ≈ 5000 Å.

The threshold characteristics of the damage process (the threshold energy and flux density) were derived in [2] from the condition that the thermoelastic stresses in the glass, which are produced around the inclusion, reach a value close to the theoretical strength of the corresponding material, which is of the order of 0.1 E (E is Young's modulus).

The theory of the interaction of laser radiation with opaque inclusions was developed within a narrower and specific framework in [3-7]. In [3-5], just as in [2], the interaction was considered in the linear approximation, i.e., at an intensity-independent absorption coefficient of the inclusion. According to estimates by Bloembergen [5], in the stationary regime the threshold damage field is $2 \cdot 10^5$ and $2 \cdot 10^6$ V/cm at dielectric inclusions measuring 10^{-5} and 10^{-6} cm, respectively. Since the latter field value coincides with the threshold field for avalanche ionization, Bloembergen [5] regards inclusions of 10^{-6} size as not dangerous.

In [6-7] account was taken of the exponential temperature dependence of the absorption coefficient of the surrounding dielectric medium. It was shown that despite the smallness of the dielectric absorption, the distribution of the temperature around the absorbing inclusion is unstable. The threshold of this instability was calculated in [6], and the time of its development was calculated in [7]. Numerical estimates [6-7] show that for an inclusion measuring 10^{-5} cm, a laser pulse duration 10^{-3} sec, and a forbidden-band width ≈ 5 eV the threshold field is $\approx 10^6$ V/cm. This electric field intensity is close to the threshold of impact ionization, so that the degree to which the actually observed damage threshold can be determined by the thermal-ionization mechanism remains unclear.

2. Damage Due to Absorption of Energy by the Electrons in Avalanche Ionization

Avalanche impact ionization by free electrons is one of the main mechanisms that can determine the maximum optical strength of impurity-free transparent dielectrics acted upon by laser pulses. Enough experimental research has been performed by now [8-14] on this question. It was shown that in nanosecond laser pulses the threshold of avalanche ionization is of the order of 10^9-10^{10} W/cm^2. Avalanche ionization in an optical field was considered theoretically in [9, 15-19].

According to the prevailing notions, damage produced by impact ionization is due to the unlimited growth of the concentration of free carriers, which in turn leads to an increase in the rate of energy input to the lattice.

From the theoretical point of view, two different problems can be considered:

1. Problem of Instability in the Electron System. In the stationary state, the concentration of the free carriers is determined from the equation [20]

$$N\{\bar{w}_i(\varepsilon, T) - \bar{w}_r(\varepsilon, T)\} + N_0(\varepsilon, T) = 0, \tag{6}$$

where $\bar{w}_i$ (ε, T) and $\bar{w}_r$ (ε, T) are the probabilities, averaged over the distribution function, of the impact ionization and recombination; N_0 (ε, T) number of carriers of a given type, produced per unit time in a unit volume as a result of photoionization and thermoionization; ε, electric field intensity; T, temperature. $\bar{w}_r$ decreases and $\bar{w}_i$ increases with increasing field. This is due to the fact that, as a rule, it is the slow electrons that recombine and the fast ones produce the impact ionization. With increasing field, the distribution function is so deformed that the number of slow electrons decreases and the number of fast electrons increases. In a field ε_g, in which $\bar{w}_i = \bar{w}_r$, the carrier density N determined from (6) becomes infinite. This means that there is no stationary state and an electron avalanche develops. Therefore, if the laser pulse is long enough, the breakdown threshold is determined by the condition $\varepsilon > \varepsilon_g$.

2. Problem of the Time Evolution of the Electron Avalanche. In short laser pulses the condition $\varepsilon > \varepsilon_g$ may be satisfied but no breakdown occurs, since the electron avalanche may not have sufficient time to reach the breakdown stage. In this sense the condition $\varepsilon > \varepsilon_g$ is necessary but not sufficient for electric breakdown. The breakdown criterion for a short pulse can be determined from the requirement that the concentration of the free carriers reach a definite value during the time of action of the pulse. As noted in [21], at an electron density 10^{18} cm^{-3} the rate of energy input as a result of absorption of the laser radiation becomes so high that the lattice temperature rise can be noticeable even during a picosecond pulse. A calculation in accordance with this scheme was carried out by Molchanov [15]. The formula derived by him leads to the following relation for the threshold field

$$\varepsilon_{cr}^2 \tau = \text{const}, \tag{7}$$

i.e., in contrast to the threshold field ε_g determined from (6), in this scheme the threshold field depends on the pulse duration. Below ε_{cr} there is a bound on ε_g, $\varepsilon_{cr} > \varepsilon_g$. The validity of (7) is bounded from above by the field value at which a substantial role is assumed by multiphoton processes [22].

3. Effect of Nonlinear Refraction

The phenomena connected with nonlinear refraction (self-focusing, defocusing, etc.), i.e., with the dependence of the refractive index of the medium on the parameters of the radiation propagating in it, have been the subject of extensive discussions in connection with the development of high-power laser installations. The self-focusing phenomenon (the principal theoretical premises and the experimental results) is described in the review paper [23], which contains also a rather detailed bibliography.

In the present section, questions connected with self-focusing and defocusing will be discussed from the point of view of laser damage, i.e., the extent to which these effects can influence the damage process.

The principal parameters of the laser damage processes, which enable us to establish the presence of one damage mechanism or another, are the threshold characteristics of the radiation, viz., the flux density or the energy density. Nonlinear refraction, by its very nature,

can cause substantial changes in the spatial distributions of the radiation parameters and consequently lead to an incorrect interpretation of the experimental results.

Nonlinear refraction can be due to various physical causes. The literature usually discusses the following: electrostriction, the high-frequency Kerr effect, and heating. The first two mechanisms of nonlinear refraction always lead to self-focusing. The last mechanism, which is connected with the dependence of the refractive index on the temperature, can lead also to the inverse phenomenon — defocusing. It appears that various combinations of these mechanisms are possible.

Since the amplitude profiles of real beams usually differ from parabolic, a substantial role can be played in the self-focusing process by aberrations. A particular case for a two-dimensional beam is considered in [23]. It is shown there that the rays approach the beam axis, self-focusing takes place, but in contrast to a parabolic profile rather strong aberrations set in. The intensity of the light reaches a (finite) maximum. The effective self-focusing length is larger than in the parabolic case.

Aberration self-focusing is apparently most typical of real beams. Although it is difficult to calculate the picture of the aberrations for each concrete case of a three-dimensional beam, it is clear that the growth rate of the field on the axis of a real beam subject to aberration will be smaller than for the case of parabolic distribution.

The relative role of various self-focusing mechanisms is discussed in detail in [24], where self-focusing and defocusing of light beams in media having weak absorption are considered. The relative role of electrostriction, of the thermal expansion that accompanies the energy absorption, and of the Kerr effect are assessed. Estimates are made of the absorption-induced divergence of an inhomogeneous beam. The effect of suppression of self-focusing by the growing defocusing action of thermal expansion is considered. It is shown how a plane wave that is unstable to field perturbations in the absence of absorption becomes stabilized as a result of the absorption.

4. Effect of Hypersound Produced in Stimulated Mandel'shtam–Brillouin Scattering

During the earlier stages of the research on laser damage, much attention was paid to still another mechanism — damage by the hypersonic wave produced as a result of the effect of stimulated Mandel'shtam–Brillouin scattering (SMBS). The results of a number of experiments [25-27], aimed at explaining the mechanism whereby transparent dielectrics are damaged by laser radiation, were interpreted as proof of the important role played by SMBS and by hypersonic waves in the onset of the damage.

The pressure produced in the hypersonic wave in the case of SMBS can be theoretically estimated by starting from the equations given in the review paper [28]. In [1], in the section devoted to a discussion of the hypersound hypotheses of laser damage, the pressure due to electrostriction is estimated at

$$|P_{st}| = \rho\left(\frac{\partial\varepsilon}{\partial\rho}\right)\frac{\mathcal{E}^2}{8\pi}. \tag{8}$$

At the intensity corresponding to the threshold of damage of glasses by laser pulses of nanosecond duration this pressure is, according to the estimate in [1], 30 kgf/cm^2. Comparing this value with the dynamic cracking stress $2\cdot10^4$ kgf/cm^2, the author reaches the conclusion that electrostriction pressure cannot play an important role in laser damage.

Nonetheless, if one speaks of the action of hypersound in SMBS, the pressure in the hypersonic wave itself must be calculated, since it can substantially differ from the striction pressure which acts as the driving force in SMBS.

If the medium is subject to sufficiently large acoustic losses at a given scattering angle, so that the following inequality is satisfied [28]

$$\tau > g/2\alpha_s v, \tag{9}$$

where τ is the duration of the laser pulse; g, stress in the entire region of nonlinear interaction; α_S, sound absorption coefficient; and v, speed of the sound, then we can use the so-called stationary SMBS theory. As an upper-bound estimate of the pressure in a hypersonic wave, this is perfectly acceptable for pulses with durations amounting to several dozen nanoseconds. If the inequality (9) is satisfied, then the pressure in the hypersound wave, at

180° scattering and exact satisfaction of the Bragg condition, is given by

$$|P| \simeq \rho\left(\frac{\partial \varepsilon}{\partial \rho}\right)\frac{\mathcal{E}^2}{8\pi}\left(\frac{\pi}{2\lambda\alpha_s}\right). \qquad (10)$$

It is seen that the expression (10) for the pressure differs from (8) in the additional factor $\pi/2\lambda\alpha_s$, which is due to resonant buildup of the hypersonic wave. For quartz at room temperature $\alpha_s \simeq 3\cdot10^2$ cm^{-1}. At the neodymium-laser wavelength the factor $\pi/2\lambda\alpha_s \simeq 50$, yielding for the pressure $|P|$ a value $\simeq 1.5\cdot10^3$ kgf/cm^2. But even this pressure is smaller by one order of magnitude than the dynamic strength of the glasses.

Summarizing the results of the present chapter, some conclusions must be drawn. First, with respect to the relative roles of the laser-damage mechanisms via heating of the strongly absorbing inclusions and via absorption of light by the electrons in avalanche ionization: At the present state of the technology of eliminating impurities from the initial components, when the optical materials used in laser technology are manufactured, the first mechanism is the most pressing, at any rate at laser pulse durations $\tau \geqslant 10^{-6}$ sec. As to the duration range 10^{-10} sec $\leqslant \tau \leqslant 10^{-8}$ sec, no unequivocal conclusions can be drawn, since the threshold of avalanche ionization coincides with the formal estimate of the threshold for the strongly absorbing inclusions. Nonetheless, the role of strongly absorbing inclusions must be taken into account both in experiments with short pulses and in discussions of the results of these experiments. Second, the following must be stated concerning the two accompanying effects discussed in Secs. 3 and 4 (self-focusing and SMBS). Self-focusing cannot be regarded in principle as a damage mechanism — it must only be taken into account in the experiments as a cause of a possible error in the estimate of the intensity. Naturally, in each concrete case it is necessary to estimate the roles of the different nonlinear-refraction mechanisms. For example, in the case of free-running lasers the principal mechanism is apparently thermal. One must not forget also the important role of aberrations in the self-focusing of real beams, which can reduce the self-focusing effect only to a negligible increase of the intensity. As to SMBS, it must be regarded at the present state of the art as a pure side effect, since both the theoretical estimates and the results of the experimental studies (especially for long pulses) show that SMBS cannot serve as a damage mechanism.

CHAPTER II

INVESTIGATION OF THE INTERACTION OF LASER RADIATION WITH TRANSPARENT MATERIALS DURING THE STAGE PRECEDING THE DAMAGE

1. Investigation of Optical Inhomogeneities Produced in Transparent Dielectrics by Laser Radiation

1. Experimental Setup and Procedure of High-Speed Interferometry in the Beam of a Laser Operating in the Regime of Repeated Giant Pulses. To investigate the optical inhomogeneities produced by the action of free-running laser radiation on transparent dielectrics, we used the high-speed interferometry procedure [29-31]. The experimental setup is shown in Fig. 1. The neodymium laser 1 consisted of a master generator (rod 20 × 240, pump 20 kJ) operating in the free-running regime, and two amplifiers (rods 20 × 240, tilted 4° each, pump 20 kJ each). The maximum output energy of such a laser reached $\simeq$ 400 J at a pulse duration $\simeq 10^{-3}$ sec. The beam divergence integrated over the time was $\simeq 5\cdot10^{-3}$ rad. It must be noted here that in view of the multimode character and fluctuating time structure of the free-running regime, intensity fluctuations in the far field are possible.

The question of spiked emission by lasers has been the subject of many theoretical and experimental studies. Nonetheless, the nature of this phenomenon is not fully clear to this day. It appears to be connected with the multimode character of the oscillations in the optical resonator. This is evidenced, in particular, by the results of a number of experiments that show that the character of the transient, for one and the same active material, depends substantially on the configuration of the optical resonator. For example, when resonators with mode selection are used, regular and damped pulsations are normally observed.

The random-pulsation regime sets in in the case of a plane-parallel Fabry—Perot resonator with relatively small distance between the mirrors (less than 1 or 2 m). To estimate the deviation of the divergence in individual pulsations from the mean value (integrated over the time), the energy distribution in the far field was investigated by a high-speed SFR-2M

camera operating in the slit-scanning regime. The time resolution in this case was $\simeq 10^{-7}$ sec. The distribution function was in no way Gaussian, apparently because several oscillation modes are generated even during one spike of the free lasing. The divergence was determined in this case on the basis of the equivalent area

$$\theta = \frac{2}{f}\left(\frac{S_{eq}}{\pi}\right)^{1/2}, \tag{11}$$

where

$$S_{eq} = 2\pi \int_0^\infty \varphi(r)\, r\, dr, \tag{12}$$

i.e., of the area of the equivalent uniformly illuminated light spot with illumination equal to the maximum illumination in the real spot; $\varphi(r)$ is the energy distribution function in the far field.

Numerical integration by formula (12) and statistical averaging over the individual lasing spikes has made it possible to establish that the excess of the intensity over the mean value, due to the divergence fluctuations, did not exceed 30%. The maximum possible value of the intensity, due to simultaneous fluctuations of the divergence and of the power, was determined from the breakdown in xenon at high pressure [32] and amounted to $\leqslant 10^8$ W/cm^2 under the conditions of this particular experiment for a lens with focal length f = 200 mm.

The radiation of the laser was focused with the aid of lens L_1 of focal length f = 200 mm into the interior of the investigated sample S. The sample, in the form of a parallelepiped measuring 30 × 20 × 10 mm, was placed inside one of the arms of Michelson interferometer 3.

The source of auxiliary illumination was a ruby laser (rod 12 240, pump 10 kJ), operating in the regime of repeated giant pulses [33]. This regime can be obtained by introducing into the resonator a nonlinear element that has resonant losses. In this particular system the nonlinear element was a plate F of KS-19 glass, 3 mm thick. The radiation of such a laser consists of a series of giant pulses of duration $(15\text{-}20)\cdot 10^{-9}$ sec and with an interval between pulses that can be adjusted in the range $(15\text{-}150)\cdot 10^{-6}$ sec. The interval could be adjusted by varying the pump energy and by selecting the initial transmission coefficient of the nonlinear element.

The ruby-laser radiation was collimated with a telescope C. The objective L_2 projected the plane passing through the optical axis of the lens L_1 onto the surface of the photographic film SF.

The frames were separated in space with the aid of the scanning-mechanism block of the SFR-2M camera. This produced on the photographic film placed in the image plane of the objective L_2 a frame-by-frame picture of the investigated process.

The spatial resolution, determined by the duration of one giant pulse of the ruby laser and by the speed of the image on the film, amounted under the conditions of our experiment to $\simeq$ 100 lines/mm. The spatial resolution of the optical system shown in Fig. 1 was determined by the choice of the objective and the photographic film. Using an objective of focal length 300 mm and "isopankhrom" 15TT-800 film, the spatial resolution in the dynamic regime was $\simeq$ 10 lines/mm.

To reduce interference patterns we used the Van Voorhis method, which yields quantitative data for the axisymmetric problem. According to this method, the transverse section of radius R is broken up into N annular zones. The function $\Delta n(r) = n(r) - n_0$, which gives the dependence of the increment of the refractive index on the running cylindrical coordinate r, where n_0 is the refractive index in the unperturbed medium, is replaced by the approximation piecewise-linear function

$$\Delta n(r) = \frac{\lambda}{\pi} \sum_{\mu=1}^{N-1} C_\mu \alpha_\mu(r), \tag{13}$$

where $\alpha_\mu(r)$ is chosen to be a function equal to zero at $r \leq r_{\mu-1}$, increasing to unity at $r = r_\mu$, and again decreasing linearly to zero in the next zone, remaining equal to zero at all $r > r_{\mu+1}$. After substituting the function chosen in this manner in the Abel integral

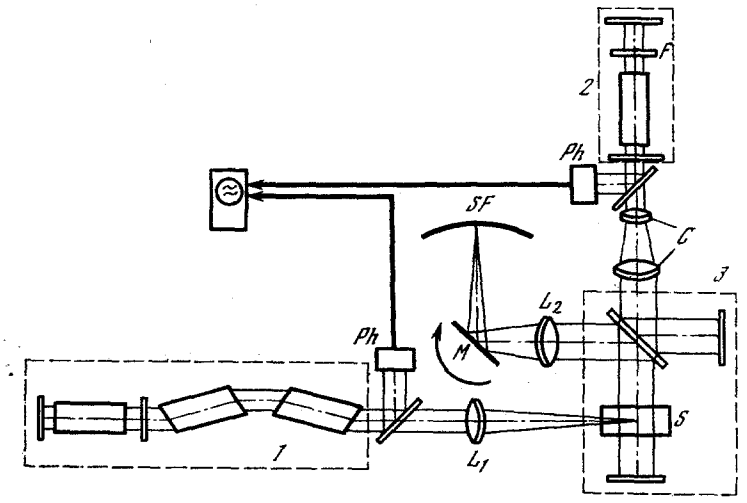

Fig. 1. Diagram of experimental setup for the investigation of optical inhomogeneities produced by the influence of laser radiation in transparent dielectrics during the stage preceding the damage. 1) Neodymium laser; 2) ruby laser operating in the regime of repeating giant pulses; 3) Michelson interferometer; S) sample of investigated material; L_1) lens that focuses the neodymium-laser radiation into the interior of the sample; L_2) lens that projects the plane of the optical axis of the lens L_1 on the photographic film SF of the high-speed camera; C) collimating telescope; M) rotating mirror; F) passive shutter (KS-19 glass); Ph) F-5 photocell.

$$S(y) = \frac{1}{\lambda}\int_{y}^{R} [n(r) - n_0]\frac{dr^2}{\sqrt{r^2 - y^2}}, \tag{14}$$

where S(y) is the relative deviation of the interference fringe from its null position, an expression is obtained for the approximate values of $\Delta n(r)$ in each zone

$$\lambda S_i/q = \Delta n_i \rho(i, i) + \sum_{\mu=i+1}^{N-1} \Delta n_\mu \rho^*(i, \mu), \tag{15}$$

where λ is the wavelength; S_i, relative deviation of the interference fringe in the i-th band; q, width of the band, $\rho^*(i, \mu) = \rho(i, \mu m) - \rho(i, \mu - 1)$. The coefficient $\rho(i, \mu)$ is given by

$$\rho(i, \mu) = (\mu + 1)\sqrt{(\mu+1)^2 - i^2} - \mu\sqrt{\mu^2 - i^2} - i^2 \ln\frac{\mu + 1 + \sqrt{(\mu+1)^2 - i^2}}{\mu + \sqrt{\mu^2 - i^2}}. \tag{16}$$

If a sufficiently complete set of coefficients $\rho^*(i, \mu)$ is available, it is possible to reduce the determination of Δn_i to calculations in tabulated form. Special attention must be paid here to the sources of the errors that arise in the reduction of the interferograms. In addition to the deviations of the real physical conditions from the ideal ones and the observation errors, it is necessary to add the errors due to replacement of the mathematical limiting process by the approximate finite mathematical operations. These errors arise even when the exact and approximate functions coincide at the boundaries of the zones. The values of these errors decrease with increasing number N of the zones in proportion to $N^{-1/2}$. At the same time, the observation errors increase in proportion to $N^{1/2}$. It follows therefore that there is an optimal number of zones for the reduction of the interferograms. The estimate of this optimal number is quite difficult because this number is different even in the same optical system if the profile n(r) has different forms. Thus, for example, in [34] a computer experiment yielded an optimal number $N_{opt} = 12$ for an exponential profile, using the Van Voorhis method at a reduction accuracy $\Delta S/S = 0.1$. The error in the zeroth zone amounted

to 5.3%. It turned out also that the Van Voorhis method for an exponential profile always underestimates the results. At the same time, for third-degree parabolas the optimal number of zones is $N_{opt} = 10$ at $\Delta S/S = 0.1$, and the error is $\simeq 2\%$. The energy distribution at the focus of the lens has a rather complicated shape even for a single spike, and it is difficult to approximate it by any analytic relation. It can only be stated that the energy density decreases rapidly from unity to $\varphi(r) = 0.3$ within a circle of radius $\simeq 0.4$ mm. The rate of decrease then slows down, and $\varphi(r) = 0$ at $r \simeq 2$ mm. As will be shown later on, it is precisely inside this circle that the noticeable values of Δn are produced. Under this situation, the number of zones into which the cross section of the caustic could be broken up was limited by the optical resolution of the system. Under the condition of the particular experiment at $R \simeq 0.6$ mm we have $N = 0.6 \cdot 10 = 6$. The reduction error was far from minimal in this case, and amounted to $\pm 10\%$ at $\Delta S/S = 0.1$.

2. Experimental Results and Their Discussion. Typical interferograms of the optical inhomogeneities produced by the radiation of a neodymium laser of energy $\simeq 100$ J and pulse duration $\simeq 10^{-3}$ sec focused inside the object are shown in Fig. 2 for different instants of time.

In the reduction of the interferograms, the symmetry axis was chosen to be the optical axis of the system made up of the neodymium laser and the focusing lens L_1. The results of a quantitative reduction for the center of the caustic of the focusing lens, in the form of plots of the change of the refractive index Δn against the distance to the symmetry axis, for different instants of time, are shown in Fig. 3. It is seen that Δn at each point increases monotonically with time; the monotonicity of this growth was verified by a large number of independent measurements.

The absence of temporal correlation between the development of inhomogeneities and the spike structure of the neodymium laser radiation, operating in the free-running regime, leads to the conclusion that the mechanism of inhomogeneity formation has an integral character. By "integral" we mean in this case the following: the value of the inhomogeneity at each point at a given instant of time t_0 is determined not by the peak value of the intensity at the given point, but by the energy radiated by the neodymium up to the instant of time t_0. The most probable mechanism of this type is the onset of thermoelastic stresses resulting from the absorption of electromagnetic energy. For thermoelastic stresses to arise far from the geometrical boundaries of the sample it is necessary to satisfy two conditions.

The first condition is

$$\operatorname{grad}(kJ) \not\equiv 0, \tag{17}$$

where k is the absorption coefficient and J is the radiation flux density.

The second condition is

$$k_g \Lambda^2 T / kJ \ll 1, \tag{18}$$

where k_g is the thermal conductivity coefficient and T is the change of the temperature.

To satisfy condition (17) it suffices to ensure that the optical channel does not go beyond the limits of the investigated sample. Under the condition of the given experiment, the inequality (18) was certainly satisfied up to temperatures $\sim 10^4$°K, i.e., to temperatures of the order of the evaporation temperature. If the heating takes place without external loads or constraints, then the stress and strain tensor components are determined by the profile of the temperature and by the geometry of the heated body (for the particular material). In the case of axial symmetry, the stress and strain tensors contain only diagonal components.

In the case of a planar stress state, i.e., when the length of the cylindrical heated region is much less than the radius, the radial displacement is the solution of the boundary-value problem

$$\frac{d}{dr}\left[\frac{1}{r}\frac{d(ru)}{dr}\right] = \alpha(1+\nu)\frac{dT}{dr}, \qquad \sigma_{rr} = 0 \text{ at } r = R, \tag{19}$$

where u is the radial displacement; α, coefficient of linear thermal expansion; ν, Poisson's coefficient; σ_{rr}, radial component of the stress tensor; R, radius of the cylinder; r, running coordinate; and T, temperature.

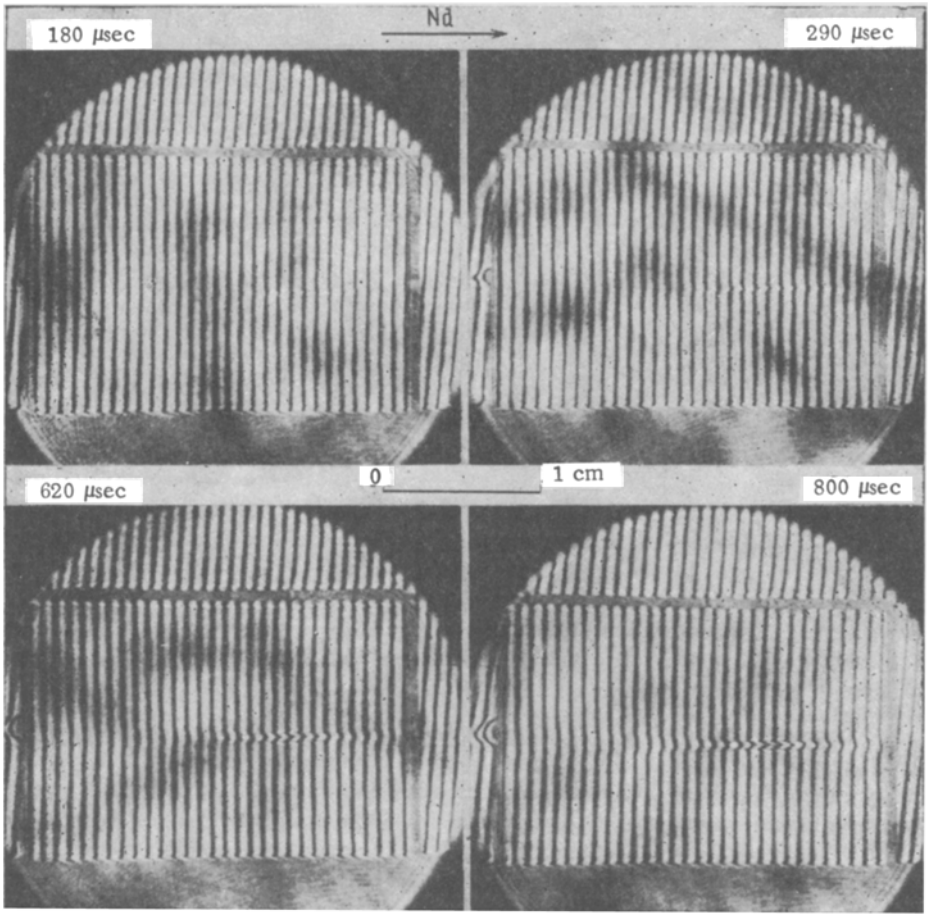

Fig. 2. Characteristic interferograms of optical inhomogeneities produced upon focusing of neodymium-laser radiation with energy $\simeq 100$ J and pulse duration 10^{-3} sec inside a sample of K-8 glass, for different instants of time. The time is reckoned from the start of a generation of the neodymium laser.

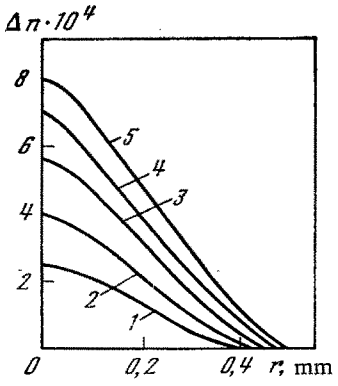

Fig. 3. Results of quantitative reduction of $\Delta n(r)$ of interferograms for the center of the caustic of the focusing lens. 1) $t = 18 \cdot 10^{7}$ sec; 2) $t = 29 \cdot 10^{7}$ sec; 3) $t = 44 \cdot 10^{7}$ sec; 4) $t = 62 \cdot 10^{7}$ sec; 5) $t = 80 \cdot 10^{7}$ sec.

The corresponding solutions for the planar deformed state, i.e., when the length of the cylinder is much larger than its radius, are obtained by replacing α by $\alpha/(1-\nu)$.

In the case of a planar deformed state, when the end faces of the cylinder are free of load, a displacement is produced also along the cylinder axis w. The corresponding displacements are given by the equations

$$u = \frac{\alpha}{r(1-\nu)}\left[(1+\nu)\int_0^r Trdr + \frac{1-3\nu}{R^2} r^2 \int_0^R Trdr\right], \tag{20}$$

$$w = \frac{2\alpha z}{R^2}\int_0^R T(r)\,r\,dr,$$

where z is the coordinate along the cylinder axis.

The components of the strain tensor take in this case the form [35]

$$\begin{aligned} u_r &= \frac{\alpha}{r^2(1-\nu)}\left[(1+\nu)\left(Tr^2 - \int_0^r Tr\,dr\right) + \frac{1-3\nu}{R^2}r^2\int_0^R Tr\,dr\right], \\ w\theta &= \frac{\alpha}{r^2(1-\nu)}\left[(1+\nu)\int_0^r Tr\,dr + \frac{1-3\nu}{R^2}r^2\int_0^R Tr\,dr\right], \\ u_z &= \frac{2a}{R^2}\int_0^R Tr\,dr. \end{aligned} \tag{21}$$

In the case of small deformations, the sum of the components of the strain tensor (21), i.e., the so-called bulk strain, is none other, accurate to second-order quantities, than the relative change of the volume

$$\left(\frac{\Delta V}{V_0}\right)^s = \frac{\alpha(1+\nu)}{1-\nu}\left[T + 4\frac{1-2\nu}{1+2\nu}\frac{1}{R^2}\int_0^R Tr\,dr\right]. \tag{22}$$

The index s denotes that the quantity pertains to the case of the stressed state. If the cylinder is uniformly heated, i.e, T(r) is constant, Eq. (22) yields the usual law of thermal expansion

$$\Delta V/V_0 = 3\alpha T. \tag{23}$$

Subtracting (22) from (23) we get

$$\frac{\Delta V}{V_0} - \left(\frac{\nabla V}{V_0}\right)^s = 2\alpha\frac{1-2\nu}{1+2\nu}\left[T - \frac{2}{R^2}\int_0^R Tr\,dr\right]. \tag{24}$$

If the right-hand side of (24) is set equal to zero, then the equation

$$T(r^*) = \frac{2}{R^2}\int_0^R Tr\,dr \tag{25}$$

makes it possible to determine r*, which corresponds to a cylindrical surface having the following property: if T(r) decreases monotonically from the axis towards the periphery, then at r < r* the substance is compressed relative to free thermal expansion, and at r > r* it is stretched; for a monotonically increasing function the situation is reversed. At r = r* the substance is deformed as in the case of free (without stresses) thermal expansion. The components of the stress tensor are then

$$\begin{aligned} \sigma_{rr} &= \frac{\alpha E}{1-\nu}\left[\frac{1}{R^2}\int_0^R Tr\,dr - \frac{1}{r^2}\int_0^r Tr\,dr\right], \\ \sigma_{\theta\theta} &= \frac{\alpha E}{1-\nu}\left[\frac{1}{R^2}\int_0^R Tr\,dr - \frac{1}{r^2}\int_0^r Tr\,dr - T\right], \\ \sigma_{zz} &= \frac{\alpha E}{1-\nu}\left[\frac{2}{R^2}\int_0^R Tr\,dr - T\right], \end{aligned} \tag{26}$$

where E is Young's modulus.

To recalculate the obtained experimental values into temperatures and stresses we must expand the expression

$$(\Delta n)^s = (\Delta n_v)^s + \Delta n_T, \tag{27}$$

where Δn_V is the change of the refractive index as a result of a change of the volume by thermal expansion, and Δn_T is the change due to the change of the temperature without allowance for thermal expansion.

To calculate Δn_V, i.e., the change of the refractive index as a result of cold tension, we can use the Lorentz–Lorenz formula

$$\frac{n^2-1}{n^2+2}V = \text{const.} \tag{28}$$

Thus, at constant T we can write

$$\frac{(n_0+\Delta n_v)^2-1}{(n_0+\Delta n_v)^2+2}(V_0+\Delta V) = \frac{n_0^2-1}{n_0^2+2}V_0. \tag{29}$$

From the relation (29) at $\Delta n/n_0 \ll 1$, $\Delta V/V_0 \ll 1$ we get

$$\Delta n_v \simeq -\frac{(n_0^2-1)(n_0^2+2)}{6n_0}\frac{\Delta V}{V_0}. \tag{30}$$

In the absence of stresses, we can rewrite (27) in the form

$$\beta T \simeq -\frac{(n_0^2-1)(n_0^2+2)}{2n_0}\alpha T + \Delta n_T, \tag{31}$$

where β is a tabulated coefficient, whence

$$\Delta n_T \simeq \left[\beta + \frac{(n_0^2-1)(n_0^2+2)}{2n_0}\alpha\right]T. \tag{32}$$

The final form of (27) for the general case of a stress state is

$$(\Delta n)^s \simeq -\frac{(n_0^2-1)(n_0^2+2)}{6n_0}\left(\frac{\Delta V}{V}\right)^s + \left[\beta + \frac{(n_0^2-1)(n_0^2+2)}{2n_0}\alpha\right]T. \tag{33}$$

In the case of an axisymmetric stress field we must substitute in (32) the value of $(\Delta V/V_0)^s$ from (22). We then obtain

$$(\Delta n)^s = \Gamma[T(r) - \bar{T}] + \beta T(r), \tag{34}$$

where

$$\Gamma = \alpha\frac{1-2\nu}{1+\nu}\frac{(n_0^2-1)(n_0^2+2)}{3n_0}, \quad \bar{T} = \frac{2}{R^2}\int_0^R Tr\,dr.$$

Equation (34) is the working formula for the calculation of the temperature. Knowing the temperature, we can calculate from (26) the components of the stress tensor. The results of calculations by this formula at r = 0, i.e., on the cylinder axis, for different instants of time t, are given in Table 1. From the data presented in Table 1 it is seen that by the end of the laser pulse σ_{zz} reaches a value close to the ultimate strength of the glass in tensor [36].

It must be noted here that the published handbook data pertain to glasses produced by the usual method without appropriate treatment. On the other hand, as long ago as the early 1930s Zhurkov [37-39], developing further the ideas of A. F. Ioffe and Griffith concerning the decisive role played by the surface in the strength of solids, obtained in investigations of glass fibers unprecedented strengths for solids, reaching $\sim 10^5$ kg/cm^2. He performed also the first experiments on the strengthening of glass fibers by chemical polishing. An estimate of the theoretical strength of a solid, from different points of view [40], turns out to be larger by several dozen times than Young's modulus, i.e., also 10^5 kg/cm^2. Since it appears that the influence of the structure of the surface can be neglected when the

TABLE 1

$t\cdot 10^6$, sec	$\Delta T°$	$\lvert\sigma_{rr}\rvert, \lvert\sigma_{\theta\theta}\rvert$, kg/cm^2	$\lvert\sigma_{zz}\rvert$, kg/cm^2
180	25	88	196
290	40	155	310
440	56	218	436
620	78	305	610
800	81	315	630

volume is acted upon by laser radiation, it becomes obvious that the stresses that develop in glass (in accordance with the table) are insufficient to produce bulk damage. Knowing the temperature ΔT, we can estimate the coefficient of abosorption of the laser radiation

$$k \simeq c_v \Delta T / W, \tag{35}$$

where c_V is the specific heat per unit volume of glass; W is the energy density at the focus. At $c_V \simeq 4$ J/cm^3·deg, $\Delta T \simeq 80°$, $W \simeq (2\text{-}3) \cdot 10^4$ J/cm^2 we get $k \simeq (1\text{-}1{,}5) \cdot 10^{-2}$ cm^{-1}. At the same time, the absorption coefficient of K-8 glass is $(5\text{-}7) \cdot 10^{-3}$ cm^{-1}. This discrepancy between those values obtained for the absorption coefficient of K-8 glass from estimates in accordance with the results of high-speed interferometry measurements and from the tabulated data may be due to two causes: either a nonlinear absorption coefficient is induced in the course of the interaction of the laser radiation with the glass, or else the quantity W in Eq. (35) is altered by effects analogous to self-focusing.

2. Investigation of the Influence of the Nonlinear Refraction on the Distribution of the Energy in the Focus

1. Investigation Procedure. The experimental setup for the investigation of the influence of nonlinear refraction that is produced in the course of the interaction of laser radiation with transparent dielectrics on the energy distribution at the focus of a lens is shown in Fig. 4.

The radiation of the neodymium laser was focused with the aid of lens L_1 of focal length f = 15 cm into the interior of the investigated sample S. The radiation was then attenuated with the aid of two plane-parallel plates P_1 and P_2 by an approximate factor 125. It was necessary to attenuate the radiation precisely in this location to prevent damage to objective L_2 (because of the large magnification, this scheme calls for the use of high-grade optics). The use of plane-parallel plates as attenuators was dictated by the fact that neutral filters, because of their large absorption coefficient, distort the distribution in the beam by formation of a thermal lens. The objective L_2 projects the image of the output end face of the sample S on the film of the camera F with a magnification of 10 times. A beam-splitting plate M_1 with reflection coefficient 50% was placed between the camera and the objective L_2. This beam-splitting plate projected the image of the end face of sample S on the slit of the high-speed photorecorder. The image of the slit was projected by objective L_3 through the rotating mirror of the photorecorder M_2 onto photographic film SF. Thus, the system made it possible to register simultaneously the time-integrated distribution of the radiation energy at the output end face of the sample S and the streak scan of this distribution. Since the energy distribution was registered from an end face of the sample, to prevent damage to the surface the neodymium-laser radiation was attenuated in such a way that the intensity at the focus was lower by a factor 1.5-2 than the threshold of bulk damage.

The photographic material was the infrared film I-1070. The determination of the region of normal density was with the aid of a nine-step optical wedge using neodymium-laser radiation. The contrast coefficient measured in this manner was 1 ± 0.1.

In connection with the conditions of the experimental setup described above, viz., in connection with the fact that when the distribution of the energy of the focus of the lens was photographed the focus was located on the surface of the sample, the question of the influence of the surface curvature due to thermoelastic stresses must be examined. The value of the z component of the displacement on the surface can be estimated from Eq. (20)

$$w = \frac{2\alpha L}{R^2} \int_0^R T(r)\, r\, dr,$$

where L is the length of the focal region.

If it is assumed that T is constant inside $r = r_0$, where r_0 is the radius of the focal spot, then

$$w \simeq \alpha T L r_0^2 / R^2. \tag{36}$$

Accordingly, the curvature radius is given by $\rho \simeq R^2/2\alpha TL$. This bending of the surface is equivalent to a planoconvex lens with focal length

$$f_\rho \simeq R^2/2(n_0 - 1)\alpha T L. \tag{37}$$

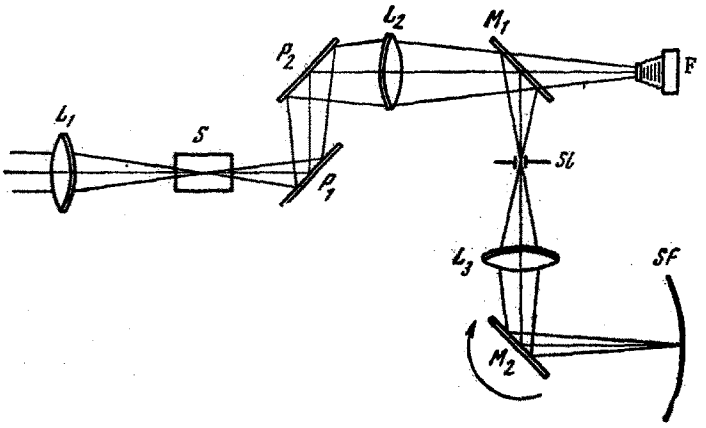

Fig. 4. Experimental setup for the investigation of the influence of nonlinear refraction. L_1) lens that focuses the neodymium-laser radiation into the interior of the sample; S) sample of the investigated substance; P_1, P_2) plane-parallel plates used as attenuators; L_2) objective that projects that plane of the output end face of the sample S on the film of the camera F and on the slit of the camera SFR-2M; M_1) beam-splitting plate with reflection coefficient 50%; Sl) slit of SFR-2M camera; L_3) objective projecting the image of the slit Sl on the photographic film in the high-speed camera; M_2) rotating mirror.

From (37) at $T \simeq 100°$, $L \simeq 0.1$ cm, and $R \simeq 1$ cm we obtain $f_\rho \simeq 3 \cdot 10^4$ cm. A lens with this focal length cannot cause significant distortions in the conditions of the described experiment.

2. Results of Experiment and Discussion. The results of the time-integrated investigation of the radiation energy distribution at the focus of the lens are given in Fig. 5. This figure shows characteristic photographs of the energy distribution for two cases. The first case (top) corresponds to photography of the distribution of the energy at a focus produced on the surface of the sample, at a flux density close to the threshold of surface damage. The second case (bottom) corresponds to the same position of the focus, but the flux density has been decreased by two orders of magnitude. That the distributions at such low flux densities in the presence and absence of a sample are identical was specially verified and it was found that at a flux density lower than the damage threshold by two orders of magnitude there are not distortions due to nonlinear refraction.

In the same figures, to the right of the corresponding photographs, are shown the results of a photometric analysis of the energy distributions. These results are represented in the form of isophots (plots of equal energy density in photographic-density units).

From the results of the time-integrated investigation of the distribution of the energy at the focus of the lens it is seen that in the case of sufficiently large (near-threshold) radiation flux density, the distribution becomes distorted. At flux densities much lower than the threshold value, the distribution of the energy has a complicated form which is apparently the result of the multimode structure of the emission of a free-running neodymium laser. When the flux density is increased up to the threshold values, the spot at the focus of the lens becomes deformed in such a way that the energy distribution becomes smoother and has a characteristic maximum at the center. The spot becomes narrower and the maximum value of the energy density increases by 1.5 times.

As already mentioned, to determine which of the mechanisms is responsible for the nonlinear refraction, slit scanning of the image of the spot at the focus of the lens was carried out simultaneously with the time-integrated measurements. The results of these high-speed measurements, in the form of the characteristic streak photographs, are shown in Fig. 6.

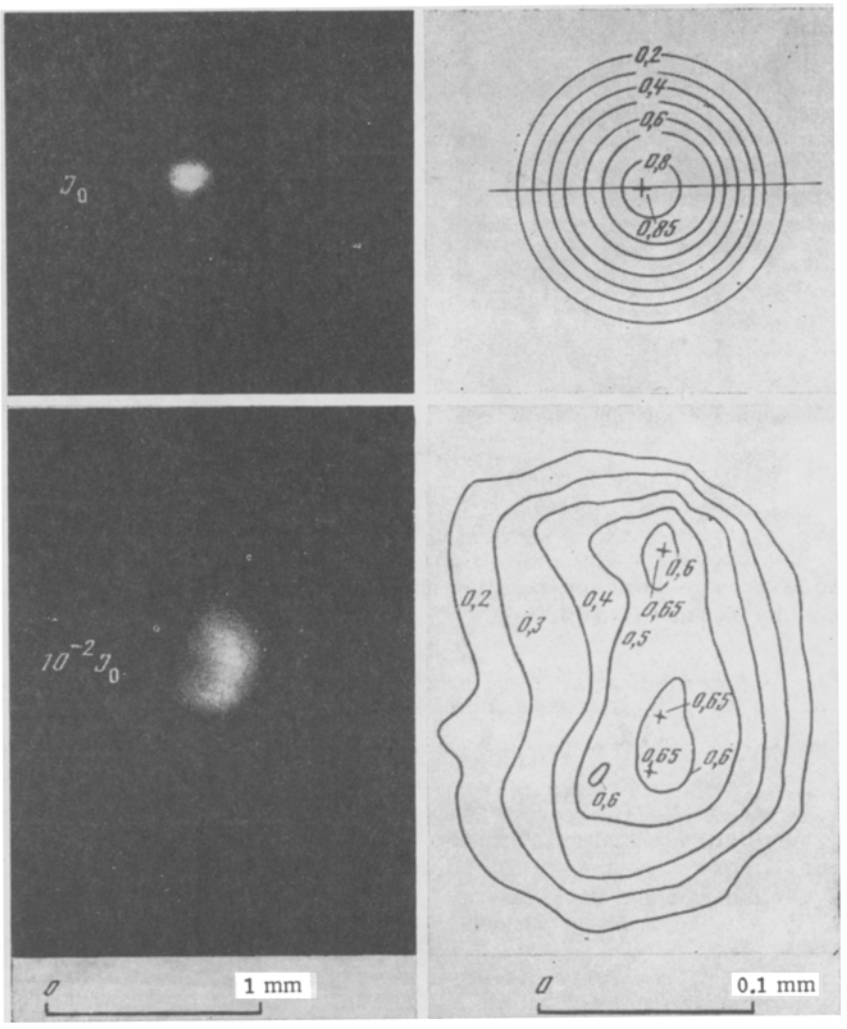

Fig. 5. Results of the investigation of the influence of nonlinear refraction (integrated with respect to time) for K-8 glass, in the form of photographs and their corresponding isophots of the radiation-energy distribution at the focus of a lens with f = 15 cm. Top) intensity of the laser radiation close to the surface-damage threshold; bottom) intensity attenuated by a factor 100.

It is seen from these streak photographs that the energy distribution at the focus becomes narrower after a time $\simeq (120\text{-}180)\cdot 10^6$ sec. The instant of time separated by such an interval from the start of the lasing is precisely the instant when distortion appears in the interference fringes (see Fig. 2). After the neodymium-laser power passes through the maximum, the distribution of the energy at the focus of the lens does not broaden and remains constant up to the end of the laser pulse.

This time evolution of the nonlinear refraction points practically unequivocally to a thermal nonlinearity mechanism.

It is also necessary to dwell in greater detail on a particular singularity of the process of distortion of the light beam as a result of nonlinear refraction, viz., that the streak photographs reveal the presence of a certain limiting (finite) dimension of the spot at the focus. The limiting dimension can be the result of the action of two competing factors. Such factors, for example, can be the formation of a thermal lens as a result of absorption of the laser energy and the resultant increase in the aberration [23].

As already noted in Sec. 1 of the present chapter, the absorption coefficients, determined from the high-speed interferometry data, differ from the tabulated value by an approxi-

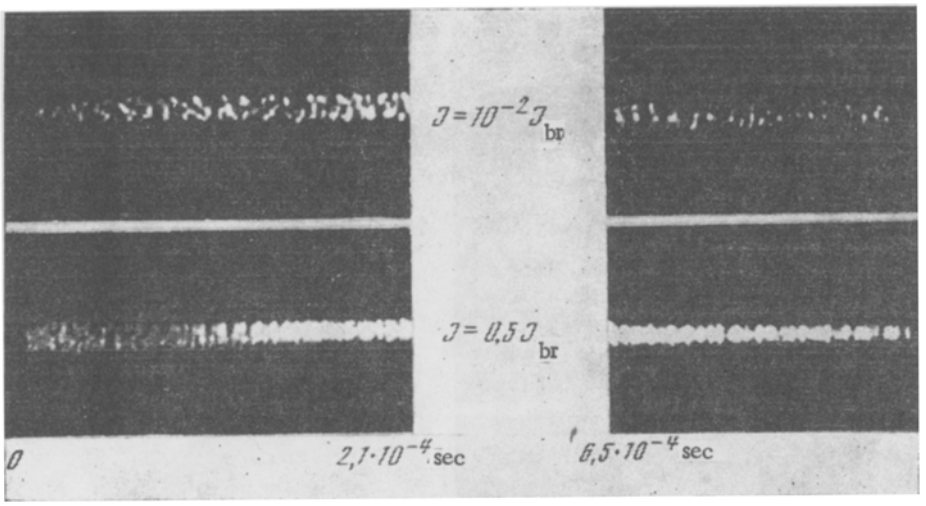

Fig. 6. Characteristic streak photographs of the radiation at the focus of the lens with f = 15 cm. Bottom) intensity close to the surface-damage threshold; top) intensity attenuated by a factor 100.

mate factor of two. The results obtained by investigating nonlinear refraction show that this discrepancy is due to the increase of the energy density, which enters in Eq. (35).

It must also be noted that analogous investigations in fused quartz have revealed the absence of any effects connected with nonlinear refraction. This fact, on the one hand, indicates that all other mechanisms of nonlinear refraction, with the exception of the thermal one, do not play a substantial role under the conditions of the experiment described above, and on the other hand, that the absorption coefficient of fused quartz is smaller by at least one order of magnitude than that of K-8.

CHAPTER III

BULK DAMAGE

1. Energy Balance

1. Experimental Setup and Procedure of Investigation with the Aid of an Integral Spherical Photometer. The experimental setup for the investigation of the energy balance in damage of transparent dielectrics by radiation from a free-running laser is shown in Fig. 7 [41, 42].

The neodymium-laser radiation was focused onto the interior of the investigated sample with the aid of lens L_1 of focal length f = 200 mm. The energy and the waveform of the incident-radiation pulse was registered with a calorimeter and with an F-5 photocell. The investigated sample was placed inside an integral spherical photometer comprising a sphere of 300 mm diameter, the inner surface of which was coated with a diffusely reflecting layer of barium-sulfide salt with a reflection coefficient 0.9. The parameters of the scattered radiation were registered with a thermopile with maximum sensitivity $\simeq 10^{-5}$ J and with an FÉU-62 photomultiplier. The waveform of the light pulse produced when the sample was damaged was registered with an FÉU-39 photomultiplier. The parameters of the radiation passing through the sample, just as at the entry, were registered with a photocell and a calorimeter.

An absolute method of determining the optical parameters of objects that scatter light in accordance with any law (i.e., having arbitrary scattering indicatrices) was proposed in 1963 by Rvachev and Sakhnovskii [43]. In the case when volume scattering is produced by the object, the intensity of the surface of a sphere with several technological openings is given by

$$J_{\text{sph}} = \frac{A\mathcal{P}}{4\pi R^2}\left\{\gamma(\theta) + \left[1 - \sum_{i=1}^{n} \frac{\gamma(\theta_i)\,\delta_i}{4\pi R^2}\right]\frac{\rho}{1-\rho'}\right\}, \tag{38}$$

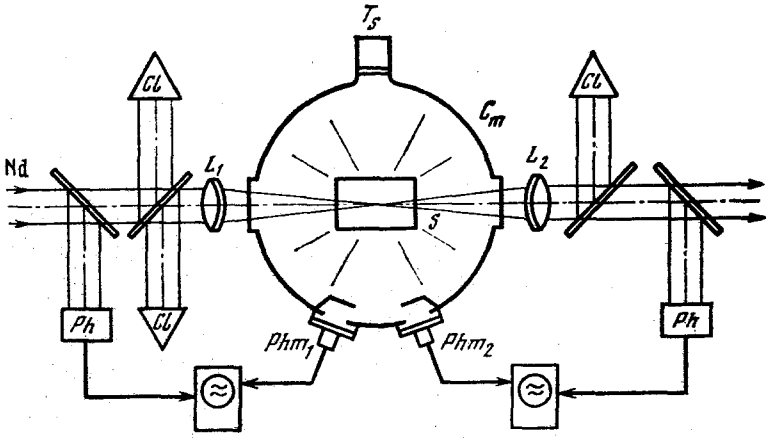

Fig. 7. Experimental setup for the investiation of the energy balance and of the dynamics of damage to transparent dielectrics by laser radiation. S) sample of investigated substance; C_m) integral spherical photometer; L_1) lens focusing the radiation of the neodymium laser in the interior of the sample; L_2) collimating lens; Ph) photocell F-5; Cl) calorimeter; T_s) thermopile; Phm_1, Phm_2) photomultipliers FÉU-62 and FÉU-39, respectively.

where $\mathcal{P}$ is the power of the incident radiation; A, scattering coefficient; $\gamma(\theta)$, scattering indicatrix; ρ, reflection coefficient of the surface of the sphere; $\rho' = \rho\,(1 - S_{op}/S_{sph})$; δ_i, area of the opening as seen from the center of the sphere at an angle θ_i; S_{op}, summary area of the technological openings; and R, radius of the sphere.

If the openings through which the scattered radiation is incident on the receiver are covered with a screen that scatters in the same manner as the surface of the sphere then the picture changes. This case corresponds to a sample located on the surface of the sphere

$$J_{sph} = \frac{A\mathcal{P}}{4\pi R^2}\left\{\frac{\pi\gamma(\theta)}{B\cos\theta} + \left[1 - \sum_{i=1}^{n}\frac{\gamma(\theta_i)\,\delta_i}{4BR^2\cos\theta_i}\right]\frac{\rho}{1-\rho'}\right\}, \tag{39}$$

where B is the equivalent solid angle of the area ΔS occupied by the sample. Since the area ΔS is part of the inner surface of the sphere, coated with a layer scattering diffusely (in accordance with Lambert's law), it follows that for this area $\gamma(\theta) = \cos\theta$, $B = \pi$, $A = \rho$ and (39) takes the simple form

$$J_{sph} = \frac{\mathcal{P}}{4\pi R^2}\,\frac{\rho}{1-\rho}, \tag{40}$$

which agrees with the formula obtained in 1920 by Taylor for the particular case of an ideally scattering surface.

It is seen from (40) that the intensity on the surface of the sphere is $1/(1-\rho)$ larger than the intensity produced by the direct rays. The quantity $1/(1-\rho)$ is called the sphere amplification coefficient.

2. Results of Experiment and Their Discussion. The calorimetric measurements have established that when the energy of the applied radiation is below threshold, there is no nonlinear absorption or scattering inside the sample (accurate to ±10%). When the damage threshold is exceeded, the observed energy increases sharply and amounts to 10-50% of the incident energy. It should be noted that the threshold radiation energy varies from experiment to experiment (by threshold energy we mean here the laser-pulse energy at which the damage took place). Thus, for K-8 glass the threshold energy ranges from 60 to 130 J. For fused quartz its value is 200-300 J.

The use of an integral spherical photometer in this experiment has made it possible to observe strong scattering when the sample was damaged. The energy of the scattered radiation remained practically unchanged at 50% of the incident energy.

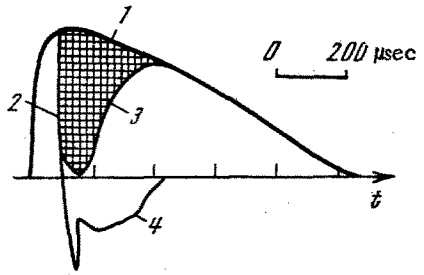

Fig. 8. Results of the reduction of the oscillograms in the form of envelopes of the pulses of the incident (1), transmitted (2), and scattered (3) radiation; the shaded area corresponds to the absorbed energy; 4) glow pulse (not to scale).

The energy passing through the sample is fluctuated within the same limits as the absorbed energy, 10-50%. The measurements have also shown that the backscattering is negligibly small, and can be disregarded in the energy balance.

Simultaneously with the calorimetric measurements, oscillograms were obtained of the waveforms of the incident, transmitted, and scattered pulses of the neodymium laser and of the waveform of the emission pulse (in the visible region of the spectrum) produced when the sample is damaged.

The reduction of the oscillograms in the form of envelopes of the pulses of the incident, transmitted, and scattered neodymium-laser radiation, referred to a single time axis, is shown in Fig. 8. The same figure shows (the amplitudes are not to scale) the self-emission pulse. The results of the statistical reduction of the oscillograms confirm qualitatively the results of the calorimetric measurements.

It is seen from the oscillograms shown in Fig. 8 that the leading front of the pulse of the transmitted radiation duplicates the front of the neodymium-laser pulse, while the trailing edge is much steeper and amounts to $(5\text{-}10)\cdot10^{-6}$ sec at the 0.7 level.

The scattered-radiation pulse has a characteristic singularity in the form of a burst — a "precursor," with duration $20\cdot10^{-6}$ sec. The position of the "precursor" on the oscillogram is such that, within the accuracy of the reduction of the oscillograms, its leading front coincides with the trailing edge of the transmitted-radiation pulse. The intensity of the scattered radiation then decreases smoothly almost to zero and this, as can be seen from Fig. 8, corresponds to an increase of the absorption coefficient in the damage zone. At $(20\text{-}100)\cdot10^{-6}$ sec later, the pulse of the main scattered radiation begins and has, as a rule, the shape of a bell with a maximum that lags the relative maximum of the incident radiation by $(200\text{-}300)\cdot10^{-6}$ sec. It is seen from Fig. 8 that the start of the glow produced when the sample is damaged coincides with the start of the scattering, i.e., with the leading front of the "precursor." The leading front of the glow pulse is slower ($\approx5\cdot10^{-6}$ sec), so that the maximum of this pulse coincides with the minimum of this scattering pulse. At the onset of the main scattering, the amplitude of the glow pulse decreases sharply (by a factor of approximately two or three) after which it drops to zero within $(200\text{-}300)\cdot10^{-6}$ sec.

A joint reduction of the oscillograms of the scattered and transmitted radiation and of the calorimetric data in the course of the determination of the damage threshold yields the following results: the energy passing through the sample at flux densities below threshold is considerably larger (sometimes by as much as an order of magnitude) than the energy passing through the sample at the instant of the damage at flux densities higher than threshold. This leads to the conclusion that the principal role in the initiation of the damage center is played not by the energy density but by the flux density of the incident radiation.

An analysis of the results shown in Fig. 8, and the correlation of the absorbed and transmitted energies, lead to following conclusions concerning the damage kinetics. The primary damage center is produced apparently within a time interval equal to the duration of the leading front of the "precursor." The details of this process cannot be analyzed because of the insufficient time resolution. The subsequent development of the damage zone can be broken up into two stages.

The first stage corresponds to the time interval during which the intensity of the scattered light decreases. This stage of the damage process consists of two stages: a first stage whose duration is equal to the duration of the trailing edge of the "precursor," and a second stage, during which the radiation is practically completely absorbed. Both stages

correspond to active development of the damage zone. The kinetics of this process is no longer connected with the primary damage center. On the oscillogram of the glow (Fig. 8), these two stages correspond to the pulse leading front during which the glow intensity increases smoothly.

The second stage corresponds to the section of the pulse of the scattered radiation, during which the intensity of the scattered light increases slowly $(200\text{-}300)\cdot10^{-6}$ sec. The absorption during this stage decreases to zero. On the oscillogram of the glow pulse, this stage corresponds to a slow decrease of the intensity. It can be shown that during this stage the activation of the interaction of the radiation with the matter stops; the radiation is merely scattered by the damage products.

Since it can be regarded as established that the damage threshold of transparent dielectrics is determined under the conditions of this experiment by the laser-radiation flux density, conclusions must be drawn concerning the causes that give rise to the damage center. To estimate the threshold flux density we can use the equation

$$J_{\text{thr}} = \frac{W_{\text{thr}}}{\tau S_{\text{eq}}}\left[1 - \Delta\frac{1-\delta}{\delta}\right]^{-1}, \tag{41}$$

where W_{thr} is the total pulse energy at which the damage took place; τ, pulse duration; S_{eq}, equivalent area of the light spot at the focus of the lens, determined from Eq. (12); Δ, depth of modulation; and δ, off-duty cycle. Substituting in this equation the mean values of the pulse parameters at which the damage took place, we obtain for K-8 glass $J_{thr} \simeq 3\cdot10^{7}$ W/cm^2 and for fused quartz $J_{thr} \simeq 5\cdot10^{7}$ W/cm^2 at $\Delta \simeq 0.5$, $\delta = 2$, $S_{eq} \simeq 10^{-2}$ cm^2. When thermal effects and the associated nonlinear refraction, which are described in Chap. II, are taken into account the threshold value of the flux density for K-8 becomes equal to $\simeq 4.5\cdot10^{7}$ W/cm^2, i.e., close to the threshold intensity for fused quartz.

As shown in Chap. I, at flux density $\sim10^{8}$ W/cm^2, such damage-center nucleation mechanism as avalanche and multiphoton ionization, which are usually discussed seriously at flux density $\sim10^{10}$ W/cm^2, cannot play a significant role under the conditions of the present experiment. The electrostriction effects can likewise be disregarded. We are left with a single mechanism that causes the damage under the conditions of the given experiment, namely the mechanism of damage via strongly absorbing inhomgeneities.

According to the theory developed in [2], a dependence of the damage threshold of transparent dielectrics on the flux density should be observed for strongly absorbing inclusions under condition (1), in which the pulse duration (for free-running lasers) should be chosen to be the duration of a single spike. The condition (1) yields in our case, for the dimensions of the metallic inclusions, a relation $R_i \ll 5\cdot10^{-4}$ cm. The corresponding critical flux densities can be estimated from the formula of [2], which yields at $R_i \simeq 5\cdot10^{-5}$ cm, for K-8 glass, $J_{cr} = J_{thr} \simeq 4\cdot10^{7}$ W/cm^2 and $\simeq 8\cdot10^{8}$ W/cm^2 for fused quartz. It is seen from these estimates that for fused quartz a discrepancy is obtained (by more than one order of magnitude) between the experimentally obtained data and the data of the theory developed in [2].

This discrepancy between theory and experiment can be explained in the following manner. At sufficiently high temperatures ($\sim5\cdot10^{3}$°K and more) the Maxwellian time becomes so small that tangential stresses may not be established, and in the calculation of the loads on the boundary between the inclusion and the matrix it is necessary to use the concept of stress rather than the concept of thermal pressure. In this approach, the coefficient of thermal expansion does not play a significant role. After all, it is precisely the difference between the coefficients of the thermal expansion of K-8 glass and fused quartz which leads to so appreciable a discrepancy between theory and experiment. If we equate the thermal pressure to the theoretical strength, i.e., 0.1 E, then the expansion for the critical flux density takes the form

$$J_{\text{cr}} = 4\cdot10^{5}\frac{k_{\text{g}}E}{\varepsilon_{\lambda}kNR_{\text{i}}}, \tag{42}$$

where k is the Boltzmann constant and N is the concentration of the particles in the solid. If we use Eq. (42), then we obtain for the critical flux densities at which damage takes place in K-8 glass and in fused quartz nearly equal values, $\simeq5\cdot10^{7}$ W/cm^2.

2. High-Speed Shadow Photography of the Damage Process

1. Shadow-Photography Procedure and Experimental Setup. If an optical inhomogeneity is placed in the path of a parallel light beam and there are no optical instruments whatever, then the images produced in this manner are called shadow images. In the same manner that the ratio $\mathcal{D}/\lambda$ ($\mathcal{D}$ is the dimension of the optical inhomogeneity and λ is the wavelength) characterizes the optical sensitivity of an interferometer system, the sensitivity of the shadow method is characterized by the magnification factor $L/\mathcal{D}$ (L is the distance between the screen or the photographic film and the optical inhomogeneity). The optical effect observed with such a sensitivity describes, accurate to within the linear approximation, the mean value of the second derivative of the refractive index. Consequently, the quantitative determination of the density in shadow photography calls for double integration and for the complicated calculations that this operation entails. It must also be added that the methods of these calculations describe least reliably precisely those phenomena which are registered most distinctly by the shadow method.

Nonetheless, shadow photography has patent advantages, which enable it to occupy a definite place in the experimental techniques alongside the more complicated methods (Schlieren photography or interferometry).

When the interaction of laser radiation with transparent dielectrics is investigated during the stage of intense damage, the shadow method is the only practical optical method, inasmuch as in the course of the damage, i.e., when cavities, cracks, etc. are formed, the resultant gradients of the refractive index are larger by several orders of magnitude than during the stage preceding the damage. Such gradients of the refractive index as, e.g., near the leading point of a moving crack, not only prevent the use of quantitative Schlieren photography, but make also the method of qualitative Schlieren photography ineffective.

The experimental setup for high-speed shadow photography (Fig. 9) [41] is similar in many respects to the setup used for high-speed interferometry. Neodymium-laser radiation whose parameters are measured with a calorimeter and a photocell is focused inside the investigated sample with the aid of lens L_1. Lens L_2, which is confocal with L_1, collimates the radiation passing through the sample; the parameters of this radiation are also registered with a calorimeter and a photocell. Just as in high-speed interferometry, the source of the probing radiation was a ruby laser generating repeated giant pulses, followed by separation of the frames on the high speed camera SFR-2M. The ruby laser radiation was registered with

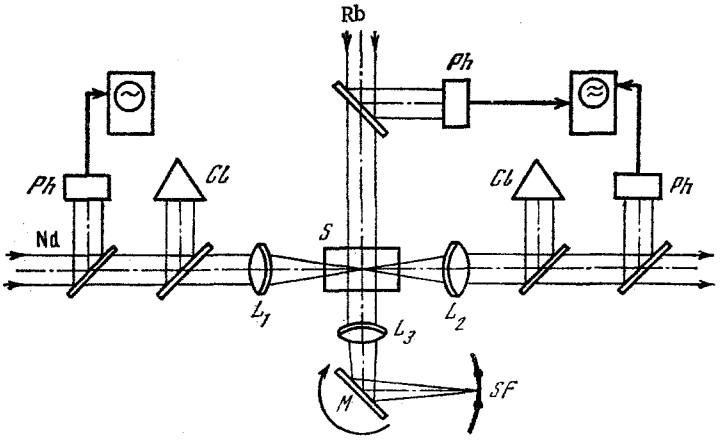

Fig. 9. Experimental setup for the investigation of the damage dynamics by high-speed shadow photography. S) Sample of investigated material; Nd, Rb) beams of neodymium and ruby lasers, respectively; L_1) lens focusing the radiation of the neodymium laser inside the sample; L_2) collimating lens; L_3) lens that projects the image of the damage zone on the photographic film of the high-speed camera; M) rotating mirror; Ph) F-5 photocell; Cl) calorimeter.

a photocell. The signal from this photocell was fed to one of the channels of a two-beam oscilloscope, while the second channel received a signal from a photocell that registered the radiation of the neodymium laser passing through the sample.

Investigations with the aid of integral spherical photometers have shown that the trailing edge of the radiation pulse passing through the sample coincides with the leading edge of the "precursor." There is therefore every reason for assuming the instant of time corresponding to the trailing edge of the pulse passing through the radiation to be the start of the damage. Thus, by recording simultaneously on a two-beam oscilloscope the giant pulses of the ruby laser and the radiation pulse passing through the sample, it is possible to fix the position of a particular shadow-photography frame relative to the start of the damage.

In approximate shadow photography, i.e., when only boundary that exists between the light and the shadow is determined, one can neglect the majority of the conditions whose violation leads to errors in the quantitative methods. Nonetheless, one condition, connected with refraction, cannot be satisfied. In all the calculation methods, an important role is played by the assumption that the light beam travels along a straight line inside the inhomogeneity. In fact the beam follows a bent trajectory. In homogeneities that bend the light beam strongly, errors can arise in the measurement of the coordinates of certain points of the object. These errors are inadmissible even in approximate shadow photography, since they can lead to incorrect estimates of the rate of motion of the boundary between the light and the shadow (e.g., the edge of a crack, etc.). To decrease the error due to displacements of the beam in the inhomogeneity plane, or to eliminate it completely, it is necessary to focus the system of the shadow instrument on the center of the investigated object. This was done in the system illustrated in Fig. 9 by lens L_3, which focused the plane passing through the optical axis of the L_1, L_2 lens system on the photographic film of the high-speed recording camera.

2. Results of Experiment and Their Discussion. The results of high-speed shadow photography of the damage of K-8 glass by neodymium-laser radiation are shown in Fig. 10 in the form of shadow photographs for different instants of time. It is seen from the shadow photographs of this figure that the damage takes in its initial stage the form of a cavity with dimensions on the order of several millimeters. Combined reduction of the shadow photographs and of the oscillograms has shown that the instant of occurrence of the cavity, within the accuracy of the reduction of the oscillogram ($\pm 5 \cdot 10^{-6}$ sec), coincides with the trailing edge of the pulse of the transmitted radiation and consequently with the leading edge of the "precursor." The damage region propagates next, in the form of a dark channel, towards the focusing lens with a velocity $\simeq 10^5$ cm/sec. During the later stage, the damage turns into one or several main-line cracks that move with velocity $\sim 10^4$ cm/sec and propagate all the way to the surface of the sample.

If we compare the results of high-speed photography with the results of oscillography of the pulses of the incident, scattered, and transmitted radiation of the neodymium laser and the glow pulse produced in the damage zone, then the evolution of the damage zone can be represented in the following form.

When the critical conditions are reached (the critical temperature and pressure) at the center of nucleation of the damage, the damage zone begins to increase rapidly in a direction perpendicular to the axis of the focusing lens. This process corresponds on the oscillograms to the leading front of the "precursor." The absorption is taken into account at the same time. The damage zone then begins to develop in a direction opposing the incident radiation, and traces a long narrow channel. Whereas the first stage, the transverse expansion of the damage zone, is caused by thermal explosion at the absorbing microinhomogeneity, the second stage, propagation towards the laser, is similar to the phenomenon of the propagation of an optical detonation wave, i.e., the motion in this direction is due to absorption of the laser radiation in a narrow front on the boundary of the damage zone. If the process of the propagation of the optical detonation wave is a pure phase process, i.e., if we can neglect the hydrodynamic motion of the matter on both sides of the detonation front, then the temperature behind the front (in the damage zone) is determined from the energy conservation law

$$T \simeq J/knv, \tag{43}$$

where J is the flux density at the focus; k, Boltzmann's constant; n, the concentration of the particles on the detonation front; and v, propagation velocity of the optical detonation wave. If it is assumed that the concentration of the particles ahead of the front is $J \simeq$

$5 \cdot 10^7$ W/cm^2 and $v \simeq 10^5$ cm/sec, in accord with the shadow-photography data, then the temperature behind the detonation front is $\sim 10^{3}$°K.

When the motion of the detonation front stops, the damage zone, as already noted, develops further in the form of cracks that propagate all the way towards the surface of the sample. This stage corresponds on the oscillograms to practically the entire time interval from the maximum of the "precursor" to the maximum of the main scattering pulse. The temporal position of this last maximum coincides with the instant of emergence of the cracks to the sample surface. The gaseous damage products then emerge to the surface and the process of active interaction is stopped.

3. High-Speed Photography of the Damage Zone

Oscillography of the glow produced when a sample placed inside an integral spherical photometer is damaged has shown that the waveform of the glow pulse has a characteristic wiggle with a maximum corresponding to the instant of the maximum absorption. Past the wiggle, the glow becomes weaker and continues all the way to the maximum of the pulse of the main scattered radiation. In connection with this characteristic structure of the glow pulse, high-speed photography was carried out of the damage zone in its own light [44, 45]. Both streak and frame-by-frame photography were used.

1. Frame-by-Frame Photography. In the frame-by-frame photography, standard front objectives I-51 and I-23 were used together with a four-stage lens adapter. At a mirror rotation speed 30,000 rpm, the frame frequency was 10^6 per second. Typical photographs of the

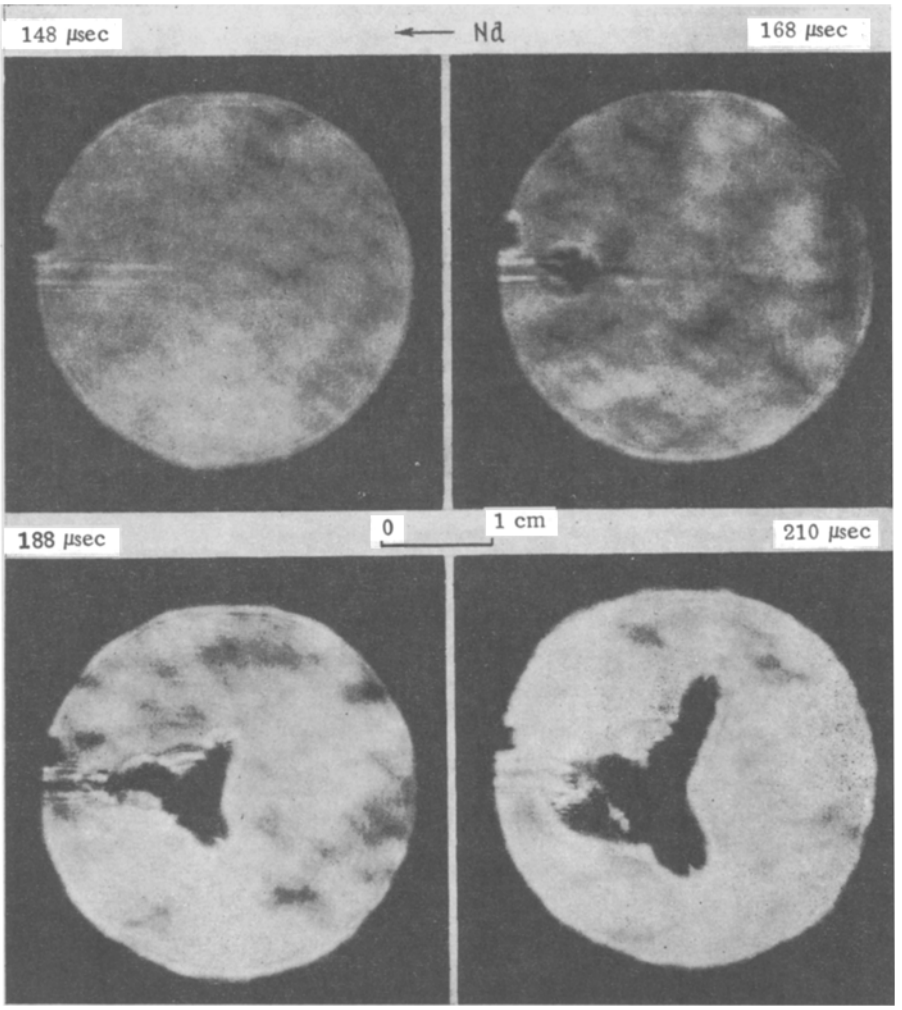

Fig. 10. Characteristic shadow photographs of damage in K-8 glass at different instants of time. The time is reckoned from the starting instant of the neodymium laser.

damage zone, obtained by photography in this region, are shown in Fig. 11. It is seen from these photographs that the damage zone constitutes a series of glowing cracks with dimension $\sim$0.1 cm, produced in succession one after the other. The glowing region duplicates the shape of the caustic of the focusing and reaches a length 3-5 cm in this direction. The process of formation of this relatively narrow and long damage zone lasts for $(10\text{-}30)\cdot10^{-6}$ sec. The damage zone propagates towards the focusing lens at a velocity $\simeq10^5$ cm/sec, i.e., the same velocity as determined with the aid of high-speed shadow photography. It should be noted here that in individual experiments the length of the damage zone reached values such that the coordinate of its last point on the optical axis of the focusing lens corresponded to a flux density approximately one-tenth the threshold surface-damage density (see Chap. IV). From the time between frames corresponding to the absence and onset of one of the cracks it is possible to determine the acceleration of the crack formation. A lower-bound estimate yields $\sim10^{11}$ cm/sec^2.

Once the damage zone starts to propagate towards the focusing lens, the damage changes (just as in the case of high-speed shadow photography) into a main-line crack that propagates all the way to the surface of the sample within a time $(150\text{-}300)\cdot10^{-6}$ sec, i.e., with a velocity $\sim10^4$ cm/sec (coinciding with the crack propagation velocity obtained with shadow photography). The instant of emergence of the main crack to the sample surface coincides, accurate to $\pm30\cdot10^{-6}$ sec, with the instant of stopping of the glow and with the maximum of the scattered-radiation pulse (as obtained with the oscilloscope). As already stated, the instant of emergence of the main crack to the surface corresponds to the cessation of the catastrophic interaction of the radiation with the dielectric.

2. Photography in the Streak Mode. The streak mode is usually used for a more accurate measurement, compared with the frame-by-frame photography, of the velocities of rather narrow glowing fronts (shock wave, detonation wave, etc.). From results of the photography in the frame-by-frame regime one can conclude that when transparent dielectrics are damaged by laser radiation the process that occurs during the first stage is qualitatively similar to propagation of a detonation front in an explosive. It is therefore of particular interest to know the velocity of propagation of such a front with the highest possible accuracy.

The optical system for the photography of the damage zone in the streak mode is shown in Fig. 12. The Dove prism PD and the objective L_1 rotate the image of the glowing region through 90° and focus it on the slit of the photorecorder. The objective L_2 and the rotating mirror M project the image in the plane of the slit onto the plane of the photographic film. At a mirror angular velocity ω rpm, the velocity of the image over the film is

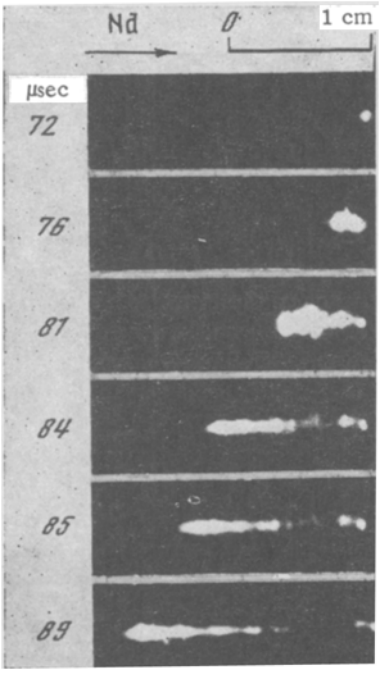

Fig. 11. Typical photographs of the glow in the damage zone for different instants of time, obtained by frame-by-frame photography with an SFR-2M camera.

$$v = \frac{\pi}{15}\omega r\left(1 + \frac{a}{r}\cos\varphi\right),$$

where r is the distance from the mirror M to the film; a, distance from the mirror rotation axis to the reflecting surface; and φ, angle of rotation of the mirror relative to the optical axis of the instrument.

The time resolution is in this case $\gamma_\tau = h/v$, where h is the width of the slit.

At a velocity $\omega = 3\cdot10^4$ rpm the linear velocity of the image over the film is $v = 1.5\cdot10^5$ cm/sec, and the time resolution at $h = 5\cdot10^{-2}$ cm is $\simeq 3\cdot10^{-7}$ sec. A characteristic photograph obtained at the indicated values of ω and h is shown in Fig. 13. It is seen from this photograph that the damage region constitutes a glowing front whose brightness attenuates rapidly with time. The diagram of its motion can be broken up into two parts. The first corresponds to a constant propagation velocity with an average value $1.5\cdot10^5$ cm/sec (the word "average" pertains to the weak pulsations on the front). The velocity then decreases smoothly to zero and the motion stops.

3. Discussion of Results of High-Speed Photography of the Glow. High-speed registration in the slit scanning mode yielded a velocity $1.5\cdot10^5$ cm/sec for propagation of the damage zone. In the case of silicate glasses, this value is well known in the physics of mechanical damage as the ultimate crack propagation velocity. On the other hand, frame-by-frame photography has shown that the damage zone consists of individual glowing cracks, and the acceleration of formation of an individual crack is estimated at $\approx 10^{11}$ cm/sec^2. The question of the limiting propagation velocities of cracks and primarily that of large acceleration is considered in the physics of mechanical damage within the framework of the theory of autocatalytic chain processes [46]. Within the framework of this theory, considering the decay of the stress field as a branched chain process that starts on the surface of the crack itself, formulas were obtained for the rate of growth of the crack. It was shown that the kinetics of the crack has two phases. The first is accompanied by large accelerations and the other one constitutes a steady-state propagation. Both phases are described by the equation for the growth rate

$$v = v_\infty(1 - e^{-t/\tau}) \Big/ \left[1 + \left(\frac{\tau_0}{\tau}\right)^2 e^{-t/\tau}\right], \qquad (44)$$

where v_∞ is the limiting propagation velocity of the crack; τ_0 is the lifetime of the "frozen" chain and is determined by the probability of breaking the chain as a result of intersection

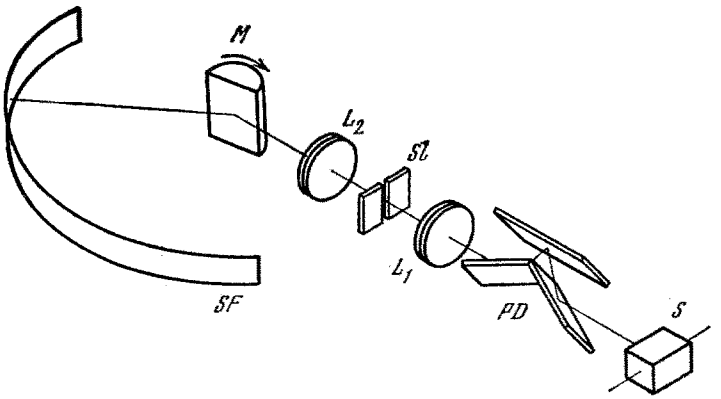

Fig. 12. Optical system for photographing a section of the damaged zone in the streak mode by a high-speed photorecorder. S) Sample of the investigated substance; PD) Dove mirror prism; L_1) objective, rotating the image of one glowing region on the plane of one streak Sl; L_2) objective, rotating the image of the streak on the surface of the photographic film SF; M) rotating mirror.

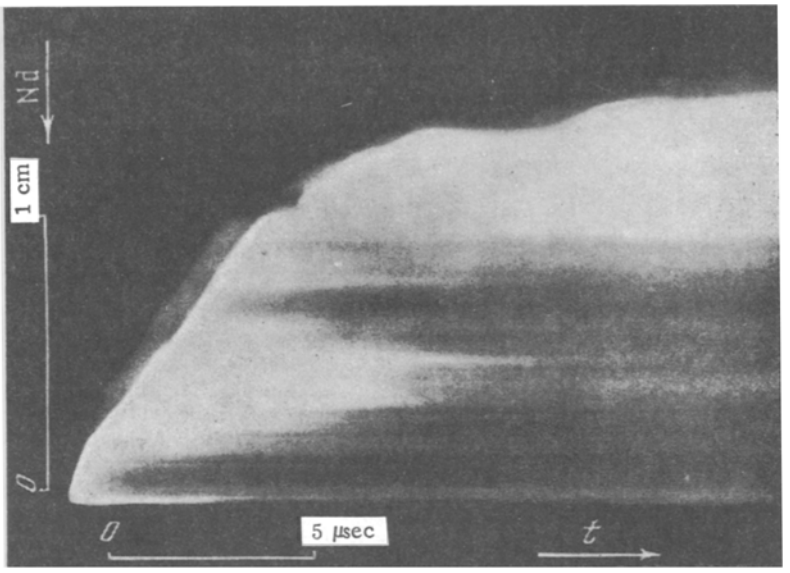

Fig. 13. Characteristic photograph of the glow of the damage zone (K-8 glass) obtained by streak photography.

and by the number of active regions that are produced per unit time as a result of relaxation fluctuations. The time τ is determined by the relation

$$1/\tau = M + \rho c/\delta, \tag{45}$$

where M is the number of active regions produced per unit time on one crack; $\rho = \sigma^2/2E$, density of the elastic energy stored in the material; c, speed of sound; and δ, specific surface energy of the crack.

It appears that greatest interest attaches to the first stage of crack propagation, where the largest accelerations are attained and the probability of branching of the crack is high.

Multiple branching of cracks was investigated in detail in experiments on mechanical damage. It was shown that accelerations $\geqslant 10^{10}$ cm/sec^2 are needed for multiple branching. It was established that such accelerations can be obtained with localized centers having a high residual-stress elastic potential (e.g., in quenched glass). Otherwise, in the absence of internal stresses, multiple branching can be produced only by an extremely high external load. Differentiating and integrating expression (44) for the velocity, we can obtain expressions for the different extremal parameters of the crack evolution (the maximum acceleration, the corresponding radius of the crack, etc.). Having, e.g., an expression for the maximum acceleration, we can estimate the average damage stress

$$\sigma \simeq \left(\frac{8E\delta a_{\max}}{v_\infty c}\right)^{1/2}. \tag{46}$$

An estimate by means of this formula for $a_{\max} = 10^{11}$ cm/sec^2 yields the value $\sigma = 80$ kg/cm^2. If we estimate the average damage stress corresponding to the start of the growth of a crack of length L by means of the Griffiths formula

$$\sigma \simeq (4\delta E/\pi L)^{1/2} \tag{47}$$

we obtain at $l \simeq 0.1$ cm a value $\sigma \simeq 100$ kg/cm^2. It can thus be stated that the quantities estimated from Eqs. (46) and (47) are of the same order of magnitude.

Since the stress estimated from (47) corresponds to a near-equilibrium state of the crack, this agreement can be apparently attributed to two causes. Either the average acceleration ($\sim 10^{11}$ cm/sec^2) estimated from the dimension of the crack and from the time interval between the frames differs from the maximum one by several orders of magnitude, or else Eq. (46), and consequently also (44), cannot be used in the present situation and an entirely different crack-development mechanism must be assumed. The experimental results favor more readily the last assumption. In fact, whereas in mechanical damage the first stage (the

acceleration of the crack) is due to avalanche-like release of elastic energy accumulated in the material by the instant of the start of the damage, in the case of laser damage this accumulated energy is known to be insufficient to damage the large volumes observed in the experiment (up to 5 cm along the caustic of the lens). The energy absorbed in the interaction volume by the instant of the start of the damage is

$$W_T = \frac{\pi}{4} J\theta^2 f^2 kht_0, \tag{48}$$

where J is the flux density in the focal region; θ, divergence; f, focal length of the focusing lens; k, absorption coefficient; h, length of the damage region; and t_0, time of the start of the damage, reckoned from the start of the lasing. The energy stored in the elastic deformation by the instant of time t_0 can be estimated from the equation

$$W_{el} \simeq \frac{2\alpha^2 E W_T^2}{\pi c_v^2 h^2 \theta D_0}, \tag{49}$$

where α is the coefficient of thermal expression; E, Young's modulus; c_v, specific heat; D_0, diameter of the spot of the lens. For K-8 glass at $\mathcal{D}_0 = 2$ cm, $J \simeq 10^8$ W/cm^2, $f = 20$ cm, $\theta = 5 \cdot 10^{-3}$, h = 5 cm, $t_0 = 10^{-4}$ sec we obtain $W_{el} \simeq 10^{-5}$ J. Inasmuch as in the case of optical glasses we are dealing with materials that are well annealed and do not contain large internal stresses, one can expect the surface energy of the produced cracks to be of the order of the energy of W_{el}. Since the specific surface energy of K-8 glass is $\delta \simeq 10^{-4}$ J/cm^2, it is seen that the stored elastic energy can result in production of only 10^{-1} cm^2 of free surface. This contradicts the experimental data (the total surface is 10-100 cm^2).

Thus, from all the arguments and estimates presented above we can conclude that to explain such large damage volumes we must resort to additional premises concerning the mechanism of crack formation and growth. One of them may be the assumption that the laser energy is converted into crack energy during the course of the crack propagation. The powerful glow observed in the course of the damage also favors this assumption.

4. Interaction of Laser Radiation with a Moving Crack

The difference between the mechanisms of interaction of laser radiation with static and moving cracks can be explained by means of experiments in which the crack is produced by an independent method, say mechanical [45]. In the case of mechanical damage, the formation of the crack usually begins on the free surface. In this case, for the laser radiation to act on the surface whose properties were not damaged by adsorbed particles of an external medium, it is necessary that the experiment be performed at vacuum or that the condition $v_{crk} - v_{av} \geqslant d/t_0$ be satisfied, where v_{crk} is the velocity of crack propagation, v_{av} is the rate of filling of the crack by the adsorbent, d is the diameter of the focusing spot, and t_0 is the instant of time corresponding to the intersection of the laser beam and the edge of the moving crack, reckoned from the instant of the production of the crack.

The following experiment was performed (Fig. 14). A steel ball SB of radius 1.5 cm was incident on the sample S of K-8 glass from a height of 200 cm. This produced an angular crack, approximately in the form of a truncated cone, that penetrated into the interior of the glass.

The laser emission was focused with the aid of a lens L of focal length f = 20 cm into the interior of the sample in such a way that the moving crack crossed the caustic of the lens. The start of the lasing of the neodymium laser and the instant of the occurrence of the crack were synchronized photoelectrically.

The ratio of the threshold intensities of the damage produced on the surfaces of static and moving cracks was determined by a suitable choice of neutral filters. The average value of this ratio under the conditions of the described experiment was equal to 2 (accurate to ±20%); this confirms, at least qualitatively, the substantial difference between the mechanism of interaction of laser radiation with the surfaces of a static and moving crack.

An increase of absorption on a freshly produced surface can result from localization of the electrons on various surface states. The origins of these states can vary. In the case of breaking of an ideal lattice, Tamm and Shockley states are produced on the surface. On a real surface, the surface stages are due to macroscopic and microscopic structure defects. All these exit if the surface is in contact with vacuum. If the surface is in contact with the

same medium, there is superimposed on this state spectrum also the spectrum of the states produced by the atoms and molecules adsorbed on the surface. The adsorbed particles can alter completely the spectrum of the surface states.

From this point of view, a freshly produced surface near the edge of a moving crack is apparently closest to the ideal case of a free surface. Even a surface produced by cleavage in ultrahigh vacuum becomes distorted after a fraction of a second by impurity and dissolved-gas atoms that diffuse from the volume.

From the theoretical point of view, the question of the band structure of a real surface remains completely answered to this day. In practice it is impossible to calculate the principal parameters of this structure, such as the concentration of the states, their positions in the band, the electron-capture cross section, and others. Experimentally, surface states were investigated relatively well only for a small group of semiconductors, such as germanium and silicon.

Thus, the question of the nature of the absorption of radiation on a freshly cleaved surface of a moving crack can be solved in parallel with the solution of the general theoretical and experimental problems of the surface states of solids.

5. Investigation of the Spectral Characteristics of the Glow Produced in Volume Damage

1. High-Speed Spectrometry Procedure and Experimental Setup. Figure 15a shows the schematic diagram of the setup for high-speed spectrometric investigation of the glow [44, 47] produced when laser radiation interacts with a transparent dielectric. The neodymium-laser radiation was focused with the aid of lens L_1, of focal length f = 15 cm, into the interior of the investigated sample. The spectrum was registered with the SFR-2M high-speed camera. The glowing region produced in the course of the damage was projected with the aid of objective L_2 and rotating mirror M_1 of the SFR-2M camera on the photographic film SF of the high-speed camera. Since the dimensions of the interaction region, at any case during the initial stage of the damage, are determined by the dimension of the caustic of the focusing lens L_1, it follows that the luminesce should trace on the photographic film a narrow glowing strip. Part of the radiation of the glowing region passes through beam-splitting plane M_2, which is a mirror with a reflection coefficient $\rho \simeq 90\%$, and is focused by the same objective onto the plane of the spectrograph slit Sl. An ISP-51 spectrograph was used in this case. The image was next projected with the aid of the objective L_3 of the collimator, the prism P_S, and the objective L_4 of the camera, with focal length 27 cm, on the photographic film of the spectrograph SF. Near the plane of the photographic film of the high-speed camera was placed a wire frame whose horizontal dimension corresponded to the height of the slit of the spectrograph. Thus, when the image of the moving region moved over the film the wire frame produced two vertical shadow lines corresponding to the time positions of the outermost points of the spectrograph slit. A streak photograph of the glowing region with the shadow lines is shown in Fig. 15b (bottom). Thus, the system shown in Fig. 15a made it possible, by recording the instant of the onset of the glow, to obtain the time scan of the spectrum within a time limited by the height of the spectrograph slit.

The obtained spectra were reduced by the method of heterochromic photometry with account taken of the spectral sensitivity of the film. This is the most general method of photographic photometry, which makes it possible to measure the relative intensities of spectral segments located in regions having different spectral sensitivities and different photographic-film contrasts. It must be borne in mind that in the measurements of the relative intensities of spectral regions that are far from one another it is necessary to take into account the possible difference in the absorption of the light by the optical system. This question can be solved by recording the comparison spectrum through the same optical system as the investigated spectrum. In this type of high-speed photography of the spectra it is necessary to take into account the deviation from the reciprocity law, i.e., account must be taken of the dependence of the sensitivity and of the contrast of the film on the exposure time. Several attempts were made to express this dependence analytically (e.g., the Schwarzschild formula), but all these attempts were inconsistent, and at the present time the deviation from the reciprocity law is customarily represented graphically. Plots of these relations are quite complicated, but their most essential feature is that starting with an exposure $\tau \leqslant 10^{-5}$ sec the characteristics of the photographic film cease to depend on the exposure. Thus, when the spectra are reduced, by choosing the width of the microphotometer slit to be $\leqslant \tau v$ (where

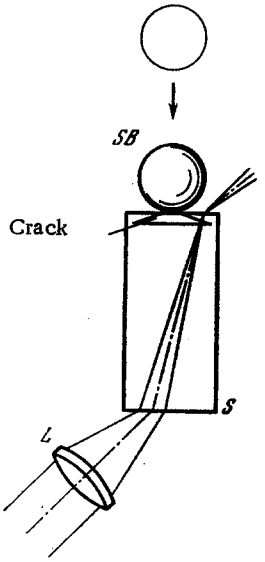

Fig. 14. Experimental setup for the investigation of the radiation of a neodymium laser with a moving crack obtained by mechanical means. SB) steel ball; S) sample; L) lens focusing the laser radiation on the surface of the crack.

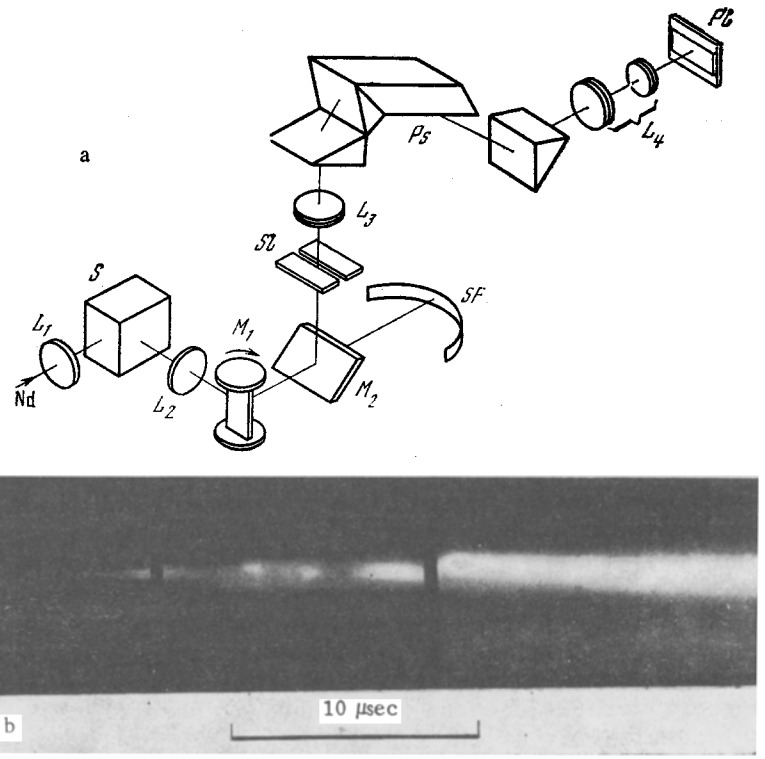

Fig. 15. Diagram of experimental setup (a) for high-speed spectrometric investigation of the glow produced when laser radiation acts on a transparent dielectric, and photograph (b) of the scan of the glowing region with shadow lines, obtained in the SF plane (below). Nd) neodymium-laser beam; L_1) lens focusing the laser radiation in the interior or on the surface of the sample; S) sample of investigated substance; L_2) lens transmitting the image of the glowing region on the surface of the the photographic film SF of the high-speed camera and on the spectrograph slit Sl; M_1) rotating mirror; M_2) beam-splitting plate; L_3) collimator objective; P_S) prism system of spectrograph; L_4) optical system of the camera of the spectrograph, with f = 27 cm; Pl) spectrographic film plane.

v is the velocity of the image on the film), it is possible to exclude the influence of deviations from the reciprocity law. This condition, naturally, imposes limitations on the source intensity and calls for appreciable velocity of the image.

The most suitable comparison source under the conditions of the described experiment is EV-45 (the Podmoshenskii source), which is a capillary discharge in a dielectric. The distribution of the intensity in the spectrum of this source corresponds to the distribution in the spectrum of an equilibrium radiation with temperature $4 \cdot 10^4$°K. The spectrum of the capillary discharge, placed at the location of the sample S, was registered through a stepped attenuator at the same speed of rotation of the mirror M_1 at which the spectra of the investigated glow were registered. To obtain the spectrograms, the "izopankhrom" 15TT-800 film was used. The comparison spectrum was reduced in steps of 100 Å, and plots of the normal density were drawn. The distributions of the relative intensities in the investigated spectra were constructed by the comparison method, i.e., by finding the intensities corresponding to the different photographic densities in the comparison spectrum and in the investigated spectra. To determine the absolute temperatures, in addition to the distributions of the relative intensities in the investigated spectra, the absolute intensities were compared at a wavelength λ = 5000 Å. The absolute temperatures were obtained by comparing the brightness and color temperatures.

2. Results of Spectrometric Investigations and Their Discussion. High-speed spectrometric investigations of volume damage have shown that the glow spectrum is continuous and retains its form at least for $(150\text{-}200) \cdot 10^{-6}$ sec, until the main crack reaches the sample surface. A typical spectrogram for fused quartz is shown in Fig. 16 (top). It is seen from the spectrogram that during the initial stage the glow in the damage region has a discrete character in time, the duration of each individual flash being $\approx 10^{-6}$ sec.

Results of the reduction of the spectrogram for fused quartz, in the form of a plot of the distribution of the relative intensities for a flash lagging the start of the damage by $3 \cdot 10^{-6}$ sec, are shown in Fig. 16 (bottom). A comparison of the data on the distribution of the relative intensities in the spectra of the emission produced in volume damage with the theoretical distribution in the black body emission spectrum, and measurement of the emissivity at a wavelength λ = 5000 Å relative to the source EV-45, has made it possible to determine the absolute temperature, which varied for the investigated samples in the range $(5\text{-}7) \cdot 10^3$°K. After the emergence of the main crack to the sample surface, the radiation spectrum becomes modified. This modification is particularly pronounced in damage of K-8 glass (Fig. 17), which contains appreciable amount of impurities. A strongly broadened inverted line

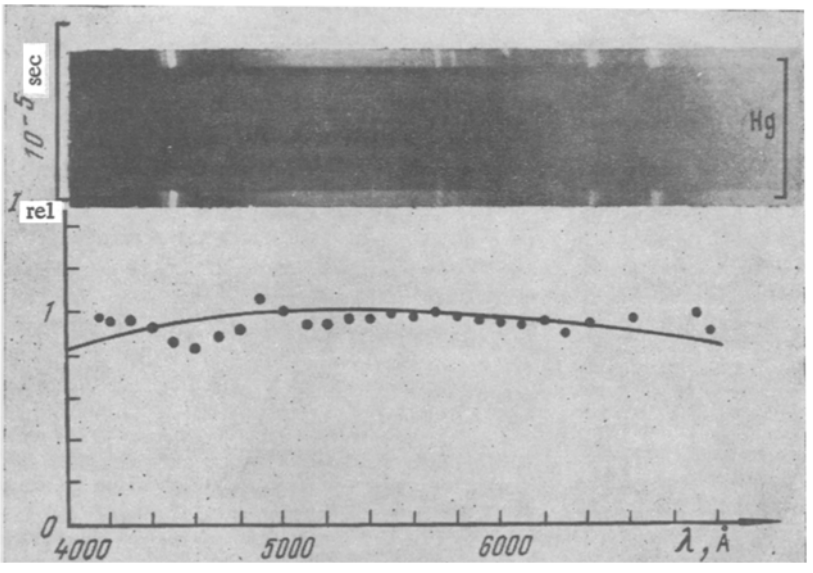

Fig. 16. Characteristics spectrogram of glow produced in volume damage of fused quartz (top) and the corresponding distribution of the relative intensities in the spectrum (bottom).

of sodium, the content of which in K-8 glass is $\approx 7\%$, appears against the background of the continuum. The continuum then gradually vanishes, the sodium line becomes narrower, and lines of other chemical elements contained in K-8 glass appear.

From the results of the measurement of the temperature in individual cracks it is seen that this temperature is close that of the phase transition (sublimation) of the damaged material. This situation can arise for two reasons: either the plasma in the cracks does not absorb radiation, i.e., it is sufficiently transparent, or else it is screened on the side of the incident radiation. The first is hardly possible at least because the conditions of the expansion of the vapor in the crack, as in a closed volume, favor an increase of the absorption coefficient because of the increased concentration. In fact, in the case of evaporation from a surface, the velocity of the evaporation wave is given according to [48] by

$$\mathcal{D} = \gamma J/\Omega, \tag{50}$$

where J is the flux density on the surface; Ω, specific sublimation energy; and γ, constant on the order of unity.

If the crack propagates at the speed of sound in a medium, then the mass of the evaporated matter by the instant of time t is

$$m \simeq (\pi/3)\, \mathcal{D}\, c^2 t^3 \rho_0, \tag{51}$$

where ρ_0 is the density of the dielectric and c is the speed of sound.

The concentration is correspondingly

$$n \simeq n_0 \left[1 + \frac{3}{\mathcal{D}} \left(\frac{\delta c}{\pi E}\right)^{1/2} t^{-1/2}\right]^{-1}, \tag{52}$$

where n_0 is the concentration of the particles in the solid.

It is seen from (52) that the concentration increases with time. The increase of the concentration n at a given temperature should lead to an increase of the electron concentration, and consequently of the absorption coefficient.

One might assume that the glow is due to the vapor of the inclusion contained in the crack and causing the onset of the crack. In this case the vapor concentration is

$$n \simeq n_0 \left(\frac{\delta}{E}\right)^{-1/2} L^{5/2} R^3, \tag{53}$$

where L is the dimension of the crack and R is the radius of the inclusion.

At $n_0 \simeq 5 \cdot 10^{22}$ cm^{-3}, L = 0.1 cm, R = 10^{-5} cm we obtain from formula (53) $n \simeq 5 \cdot 10^{13}$ cm^{-3}. At these concentrations and at a temperature $\simeq$ 5000°K the intensity of the glow would be much lower, and line spectrum would be observed, in contradiction to the experimental data (the spectrum is continuous).

From the estimates presented above we can conclude that in volume damage the glow in the cracks is due to the plasma produced as a result of evaporation of matter from the entry surface of the crack (by entry surface of a crack is meant in this case the surface through which the radiation enters into the crack). This situation can arise if a layer with an absorption coefficient close to that of a metal is located on the surface near the front tip of the propagating crack. Under the influence of the laser radiation, this layer evaporates and fills the volume of the crack, and the opacity zone moves towards the laser beam. The plasma-filled volume of the crack is screened in this case against the incident radiation, and the plasma temperature remains close to the evaporation temperature of the material ($\simeq$5000°K).

CHAPTER IV

SURFACE DAMAGE

1. Threshold Characteristics of Surface Damage of Transparent Dielectrics

Surface damage of transparent dielectrics has a number of distinguishing features compared with volume damage. First, the threshold of surface damage, unless special measures are taken (see Chap. I), is lower than that of volume damage. In the present study we measured the threshold of the surface damage of the optically strongest materials: fused quartz

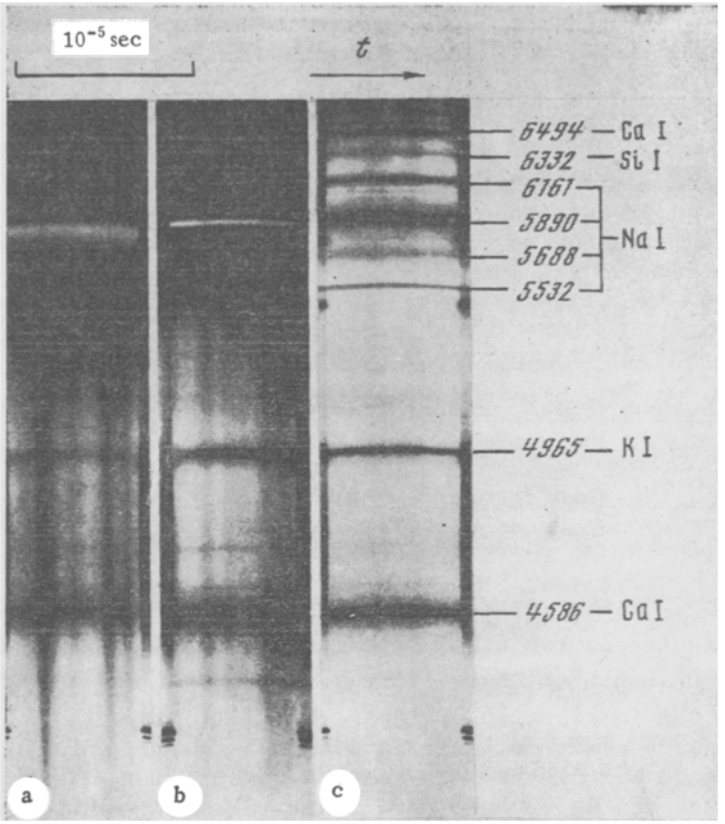

Fig. 17. Spectrograms of the glow produced in volume damage of K-8 glass during the stage corresponding to the emergence of the main crack to the surface of the sample, for different instants of time. a) $1.5 \cdot 10^{-4}$ sec; b) $2 \cdot 10^{-4}$ sec; c) $2.5 \cdot 10^{-4}$ sec; the time is reckoned from the start of the operation of the neodymium laser.

($\simeq$50 J), optical K-8 glass ($\simeq$20 J). The corresponding intensities are $\simeq 3 \cdot 10^7$ and $1.5 \cdot 10^7$ W/cm^2 for quartz and K-8 glass, respectively. Second, in contrast to volume damage, the scatter of the threshold characteristics is much lower. Whereas in the case of volume damage it reached 40-50% (see Chap. III), in the case of surface damage it did not exceed 10%, i.e., it stayed within the limits of the accuracy of the relative measurements of the laser-radiation energy.

An investigation of surface damage near threshold has shown that there are two types of damage. The first, whose threshold was measured in the present study, is accompanied by powerful optical and acoustic effects, by formation of a crater (removal of mass), and by appreciable (up to 70%) absorption of energy. The second, whose threshold is at least one order of magnitude lower than the first, is accompanied by a weak light flash (observable only with a photomultiplier) and by the cracking of the surface, in analogy with the cracking produced by contact between the surface and gas at high temperature. The characteristics of the radiation passing through the sample remain practically unchanged in this case (there is neither absorption nor scattering).

We investigated the dependence of the absorbed energy on the intensity of the incident radiation. To this end, the sample was placed inside a spherical photometer (see Chap. III). In contrast to the system illustrated in Fig. 7, the neodymium-laser beam was focused on the input surface of the sample, and the output window of the photometer was covered with a scattering screen, so that the thermopile T_S measured the sum of the scattered and transmitted energies. The absorbed energy was determined as the difference between the incident and scattered energies. Figure 18 shows a plot of the ratio of the absorbed and incident energy against the intensity of the incident radiation for K-8. It is seen from this plot that the

absorbed energy increases monotonically when the intensity is increased from the threshold value, and saturates at a level $\simeq 70\%$ of the incident energy at an intensity $\simeq 6 \cdot 10^7$ W/cm². This relation is apparently due to the structure of the focusing spot: with increasing intensity, the wings of the intensity distribution begin to be captured (begin to interact with the medium).

For an exact determination of the damage threshold of the first type, we measured the removed mass and the recoil momentum (by a free-suspension method [49]). The results of these measurements have shown that the specific removed mass $\Delta m/W_{abs}$ and the specific recoil momentum P/W_{abs} does not depend on the intensity. This confirms the assumption that the monotonic growth of the absorbed energy shown in Fig. 18 is due only to the increased area of the active interaction in the light spot. The specific removed mass and the specific recoil momentum are, respectively, $7 \cdot 10^{-6}$ g/J and 6 dyn·sec/J.

2. Gasdynamic Parameters of Plasma Flare Produced by Laser Radiation on the Surface of a Transparent Dielectric

1. Measurement of the Temperature of the Plasma Flare by High-Speed Spectrometry. The high-speed spectrometry procedure described in Sec. 5 of Chap. III was used to register the spectral composition and the dynamics of the glow of the plasma flare produced by action of the laser radiation on the surface of a transparent dielectric [44]. To this end, the laser radiation was focused with the aid of lens L_1 (see Fig. 15) on the surface of sample S. To register the spectra in the course of expansion of the flare in the vacuum, the sample S was placed in a vacuum chamber at a pressure of 10^{-2} torr.

In the course of the interaction of the laser radiation with the surface of transparent dielectrics, the produced crater is similar to that in opaque substances. Since the gasdynamic conditions inside and outside the crater are different if the focusing is sharp enough, the emission spectra were registered separately in these regions.

The characteristic spectrograms of the crater and flare emission are shown in Fig. 19 for fused quartz in vacuum. These spectrograms differ substantially from those of the glow produced in volume damage. First, these are line spectra and only at individual instants of time are continuous-spectrum bands interspersed. Second, the lines correspond mainly to singly and doubly ionized silicon and oxygen atoms, whereas when the main crack emerges to the surface of the sample (volume damage) only the lines of excited atoms were observed. This difference itself already indicates that different gasdynamic and thermodynamic conditions obtain in volume and surface damage.

Furthermore, the spectrograms of Fig. 19 demonstrate the difference between the flare and crater spectra. In the crater the bands of the continuous spectrum predominate and the lines are practically nonexistent or are very weak.

Figure 20 shows the results of the reduction of the spectrograms of the flare and of the crater in the form of plots of the distributions of the relative intensities in the continuum bands. Figure 20 shows also for comparison plots of the distributions of the relative intensities in blackbody emission spectra at temperatures $2 \cdot 10^4$ and 10^4°K, respectively. A comparison of the emissivity of the flare and of the crater with the emissivity of a comparison source of wavelength $\lambda = 5000$ Å has made it possible to determine the absolute temperatures, viz., $2 \cdot 10^4$°K and 10^4°K in the crater and in the flare, respectively.

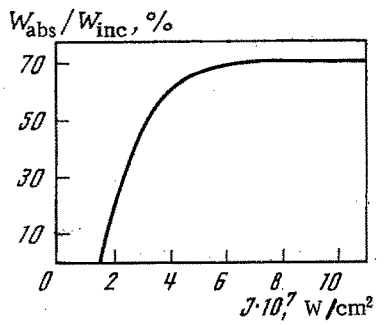

Fig. 18. Plot of the energy absorbed in surface damage of K-8 glass against the intensity of the laser radiation. The radiation was focused by a lens with f = 7.5 cm.

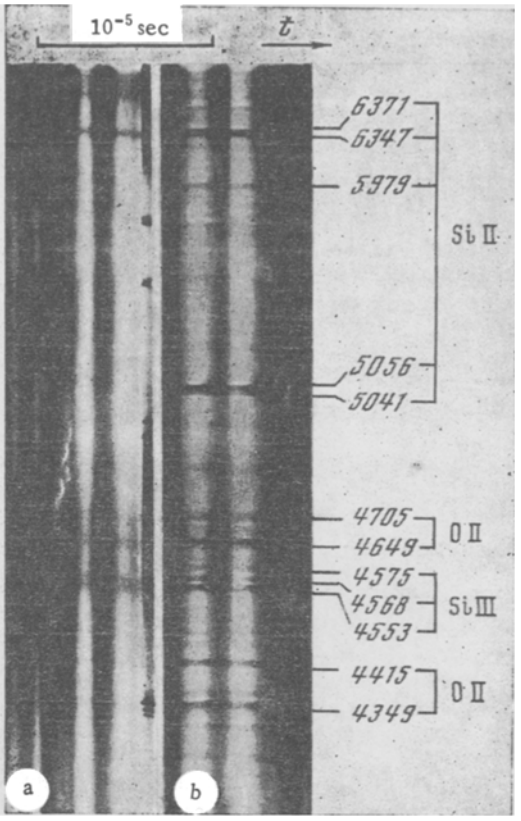

Fig. 19. Spectrograms of the glow produced by surface damage of fused quartz. a) Crater; b) flare.

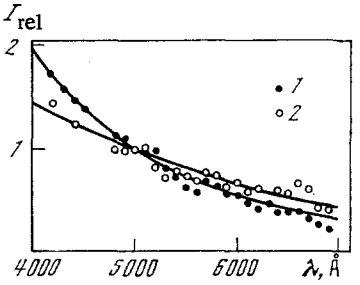

Fig. 20. Distribution of the relative intensities in the spectrum of the emission produced when fused quartz is damaged. 1) Crater, 2) flare.

Such high temperatures ($\simeq$20,000°K) of the plasma produced in surface damage suggest that the process of the interaction of the laser radiation with the surface of a transparent dielectric, during the stage of advanced evaporation, is analogous to the process of the interaction of laser radiation with a metal surface. It we assume this analogy to be a fact, then we can conclude that the absorption coefficient induced near the surface in the course of the interaction with the radiation can be comparable with the absorption coefficient of metals, i.e., $\sim 10^5$ cm^{-1}. As shown in [50, 51], temperatures $\sim$20,000°K can be produced only in absorption of the emission from the expanding plasma itself, i.e., when the so-called screening sets in. The gist of this phenomenon consists in the production of a high-temperature ionized laser that absorbs the incident radiation near the irradiated surface (when definite critical conditions are reached).

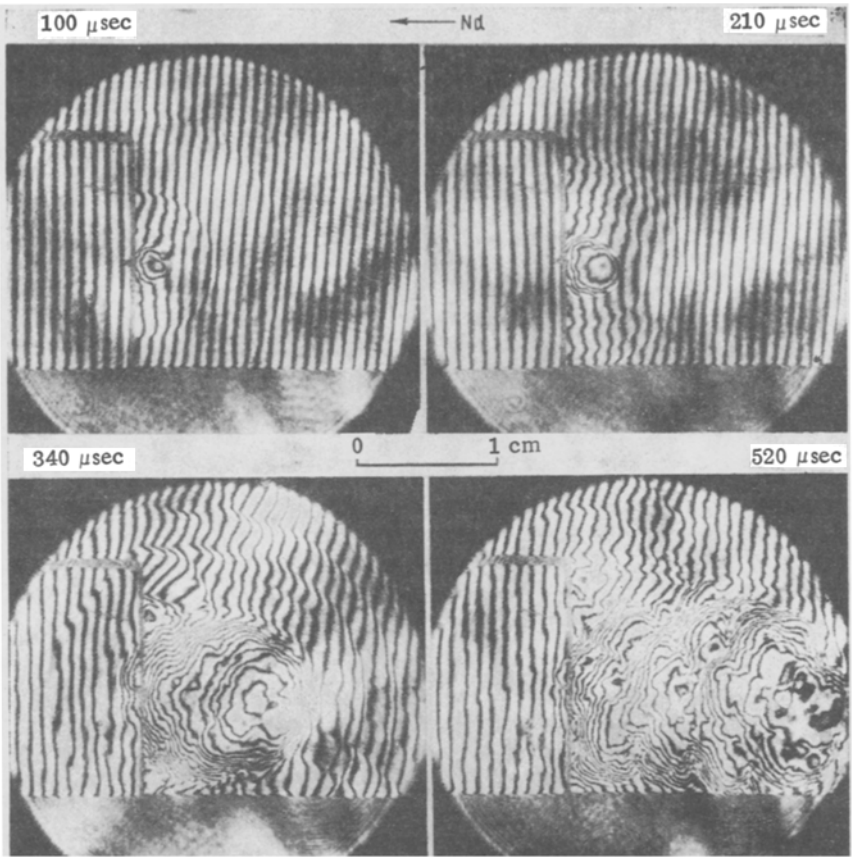

Fig. 21. Interferograms of flare produced by the action of laser radiation on the surface of K-8 glass, at different instants of time. The time is reckoned from the startup of the neodymium laser.

2. Investigation of the Motion of the Flare by High-Speed Interferometry. The procedure of high-speed interferometry in the beam of a ruby laser that generates repeated giant pulses, described in Chap. II, was used to investigate the motion of the plasma flare produced in surface damage [29-31]. In the setup illustrated in Fig. 1, the neodymium-laser radiation was focused on the surface of the investigated sample S.

The characteristics of the interference patterns of the flare for different instants of time are shown in Fig. 21. It is seen from these interferograms that during the initial stage ($\simeq 10^{-4}$ sec) the flare is close to spherical in shape, and then, as the crater becomes deeper, the flare stretches into a jet that moves in a direction opposite to the incident radiation. It is also seen that the later stage is accompanied by strongly developed turbulence.

The individual rather powerful spikes of a free running neodymium laser produce shock waves. From the interferograms of the initial stage one can estimate the average velocity of these waves, $\simeq$ 420 m/sec, corresponding to a Mach number $M \simeq 1.23$. It is difficult to estimate the shock-wave velocity during the later stage, inasmuch as during this stage its front is distorted as it moves over the strongly turbulent plasma of the flare.

Knowing the Mach number we can estimate the temperature, pressure, and density in a weak shock wave. Assuming the adiabatic exponent to be constant and equal to $\varkappa = 7/5$ in the case of a diatomic gas (it is assumed that the vibrational degrees of freedom do not play any role), we get [52]

$$\Delta T = \frac{T_0}{36}(1-\mu^2)(7\mu^2+5), \tag{54}$$

where T_0 is the temperature of the gas ahead of the front. At $\mu = 1.23$ we get $\Delta T \simeq 50$. Similarly, for the discontinuities of the pressure and density we have $\simeq 0.7$ kg/cm^2 and $\Delta\rho \simeq 0.4\,\rho_0$, where ρ_0 is the density of the air ahead of the front.

As already stated, during the initial stage of flare expansion the turbulence is weak. During this stage, assuming central symmetry and averaging the deviations of the interference fringes over the weak turbulent pulsations, we can obtain quantitative information on the distribution of the refractive index in the plasma. The interference patterns averaged in this manner for two instants of time are shown in Fig. 22. Results of a reduction of these average interference patterns by the Van Voorhis method, in the form of plots of the change of the refractive index Δn against the radius r (the symmetry center is taken to be the focal point) are shown in Fig. 23.

Interpolating on Fig. 23 the amplitude of the shock wave $(n - 1)$ on the ordinate axis, we can calculate the density discontinuity from the equation

$$\Delta\rho = \rho_0 \frac{n - n_0}{n_0 - 1}, \tag{55}$$

where n is the interpolation point on the ordinate axis and n_0 is the refractive index of the air under normal conditions. Linear interpolation yields $(n - n_0) = 0.8 \cdot 10^{-4}$, which corresponds to a density discontinuity, calculated from equation (55), with a value $\Delta\rho \simeq 0.27\ \rho_0$. If account is taken of the error in the calculation of the average velocity in the linear interpolation, then the agreement between the values of $\Delta\rho$ obtained by these two methods can be regarded as satisfactory.

Since the interferometry was carried out at a single wavelength, to be able to calculate from the measured values of Δn the concentration of the particles in the flare and the degree of ionization, it is necessary to use spectroscopic data. According to these data, the temperature in the flare is $\simeq 10^{4}$°K. Using this temperature, we can calculate the particle concentration and the degree of ionization by solving a system of two equations. The first is the Saha equation (in the region of the first ionization):

$$N \frac{\alpha^2}{1 - \alpha^2} = AT^{3/2} e^{-I/T}, \tag{56}$$

where α is the degree of ionization; N, concentration; T, plasma temperature in eV; I, ionization potential; and $A = 6.06 \cdot 10^{21} \text{cm}^3 \cdot \text{eV}^{-3/2}$. The second equation can be chosen to be the relation between the refractive index of the plasma and the concentration of the electrons and neutral particles:

$$n - 1 = a_1 N_e + a_2 N_m, \tag{57}$$

where $a_1 = -2\pi e^2/m\omega^2 = 2.16 \cdot 10^{-22}$ cm^3. The coefficient a_2 can be estimated knowing the polarizability of the atoms contained in the plasma. Assuming that the plasma contains only oxygen and silicon atoms (as the product of the dissociation of the SiO_2 molecules) and using the values of the static dipole polarizabilities of these atoms [53], we get $a_2 \simeq 2 \cdot 10^{-23}$ cm^3. A numerical solution of the system (56) and (57) at r = 0 yields $\alpha = 8 \cdot 10^{-2}$, $N \simeq 5 \cdot 10^{19}$ cm^{-3}. The electron concentration is correspondingly $N_e \simeq 4 \cdot 10^{18}$ cm^{-3}.

It should be noted that the errors in such calculations are determined mainly by the error in the coefficient a_2, which in turn depends on the accuracy of the static dipole polarizabilities of the atoms that make up the investigated gas. Thus, according to the data of [53], the experimentally obtained static dipole polarizability of silicon is $4.2 \cdot 10^{-24}$ cm^3. A deviation of ±30% from this value changes the concentrations N by almost a factor of 2.

3. Kinetics of Interaction of Laser Radiation with the Surface of the Transparent Dielectric during the Stage of Advanced Evaporation

On the basis of the results of the reported experimental investigations (see Secs. 1 and 2 of the present chapter) we can draw the following conclusions:

1. The threshold of surface damage is determined by the intensity of the laser radiation. During the stage of advanced evaporation, the interaction with the substance takes place only in that part of the light spot which lies inside a circle of radius $r(J_{thr})$, where J_{thr} is the threshold intensity of the surface damage (for comparison: in the case of volume damage the radiation is completely absorbed regardless of the excess above the threshold at the center of the light spot).

The damage (the removal of mass) takes place practically in each individual spike of the free-running lasing. This indicates that whereas the primary absorption act (in the first

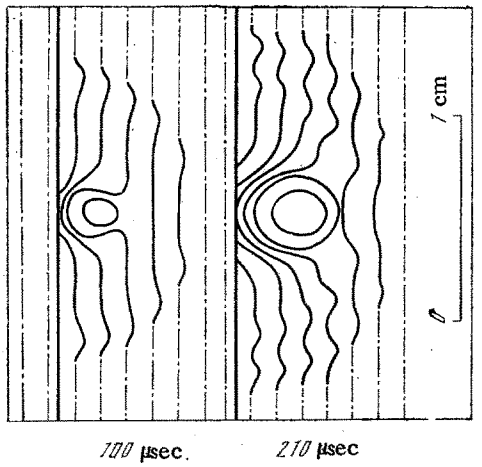

Fig. 22

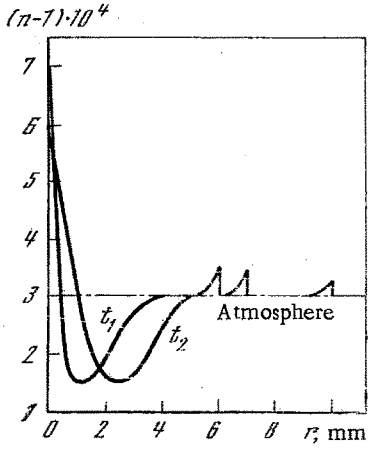

Fig. 23

Fig. 22. Flare interferograms averaged over weak turbulent pulsations.

Fig. 23. Plots of the changes of the refractive index against the radius r in a flare for $t_1 = 10^{-4}$ sec and $t_2 = 2.1 \cdot 10^{-4}$ sec.

spike with excess of J_{thr}) is due to technological contaminations or adsorption, during the stage of advanced evaporation there exists a mechanism that maintains the absorptivity of the surface that has been rid of these defects.

2. The conditions during the stage of advanced evaporation are analogous in many respects to the evaporation from the surface of a metal [50, 51]. The temperature and concentration of the electrons in the plasma flare produced as a result of the evaporation corresponds to the "screening" regime, i.e., to the regime wherein the flare plasma absorbs to a considerable degree the irradiation and screens the surface of the dielectric. This is confirmed also by the results of measurements of the specific recoil momentum and of the removed mass, from which it is seen that the values of these parameters do not correspond to the regime of transparent vapor [49] (the mass is smaller by one-half, and the momentum is practically equal to that calculated for this regime).

Starting from the foregoing, we can describe the advanced evaporation of matter from the surface of a transparent dielectric in accordance with the following scheme:

a) The primary act of absorption of the laser radiation, connected with the presence of an absorbing surface layer in the form of individual particles that were left after polishing (technological contaminations), or in the form of a layer of substances adsorbed from the atmosphere.

b) Heating of the plasma produced upon evaporation of the primary absorbing layer, to a temperature $2 \cdot 10^4$°K. The ultraviolet photons with energy equal to or larger than the width of the forbidden band of the dielectric, which are radiated by such a plasma, transfer the electrons from the valence to the conduction band. The number of such photons can be calculated from the formula

$$N = \int_{\nu_0}^{\infty} q^{\nu} \varkappa^{\nu} d\nu, \tag{58}$$

where q^{ν} is the unilateral spectral flux for photons with energy $h\nu \gg kT$ (the Wien formula); $\varkappa^{\nu} = \varkappa_0 \exp\left\{\frac{\nu - \nu_0}{\nu_0}\right\}$, spectral coefficient of absorption; and ν_0, edge of the absorption band of the dielectric ($\varkappa_0 \simeq 1$. cm^{-1}). After integrating, we get

$$N = \frac{2\pi\nu_0^2 kT}{hc^2} \varkappa_0 (1 - \varkappa_0 x) e^{-h\nu_0/kT},$$

where x is a coordinate measured from the surface to the interior of the sample. At x = 0, kT = 2 eV, this expression yields for fused quartz $N \simeq 10^{23}$ photons/$cm^3 \cdot$sec. Since the life-

time of the electron in the conduction band is 10^{-8}-10^{-9} sec, the ultraviolet photons can ensure a stationary concentration 10^{15} cm^{-3} of the free electrons. At this concentration the absorption coefficient is 10^{-3} cm^{-1}, i.e., it is comparable in order of magnitude with the absorption in the nonirradiated glass. It must therefore be assumed, as was done in Sec. 4 of Chap. III, that on the surface, near the bottom of the conduction band at $\Delta u \leqslant h\nu_L$, where ν_L is the emission frequency of the neodymium laser, there are unoccupied surface states (Tamm or Shockley levels). In the presence of ultraviolet radiation, such states will be filled with electrons from the conduction band. Since the concentration of the surface states and the lifetime of the electrons in them cannot be calculated (for reasons indicated in Sec. 4 of Chap. III), the last stage of the proposed scheme of the process of advanced evaporation from the surface of a transparent dielectric can be described only qualitatively.

c) The laser radiation causes the electrons to go from the levels $\Delta u \leqslant h\nu_L$ to the conduction band, as a result of which the stationary concentration of the free electrons becomes sufficient ($\sim 10^{17}$ cm^{-3}) to initiate thermal breakdown. Thermoionization sets in and the absorption coefficient grows avalanche-like to values 10^5-10^6 cm^{-1}. The surface temperature reaches the evaporation temperature, and the process is repeated in accordance with the described scheme.

In conclusion, we present a brief summary of the results.

1. A high-speed interferometry procedure was developed for the investigation of rapid processes.

2. The high-speed interferometry procedure was used to register optical inhomogeneities produced in glass under the influence of laser radiation during the stage preceding the damage. The values of the components of the stress tensor and the temperature in the interaction zone were determined.

3. It was shown that in the course of interaction a stable thermal lens is produced in the volume of the investigated sample and corrects the distribution of the laser-radiation energy. The time of formation of the stable lens effect is measured.

4. The energy balance of the laser radiation in the course of damage was investigated. It was established that a decisive role in the course of the nucleation of the damage center is played by the intensity of the laser radiation. The thresholds of volume damage were measured for K-8 glass and fused quartz.

5. The kinetics of the volume-damage zone was investigated by high-speed shadow photography.

6. In the investigation of the emission by using a high-speed streak camera SFR-2M it was established that the damage zone constitutes a continuous sequence of luminous cracks that propagate in a direction opposite to the incident radiation with the maximum rate of branching of the cracks in the glass.

7. A mechanism was proposed for the development of the damage zone. The control experiment was performed to determine the interaction of the laser radiation with a moving crack; the results of the experiment have confirmed the proposed mechanism.

8. The spectral characteristics of the emission of the volume-damage zone were investigated. The temperature of the plasma filling the cracks was measured.

9. A comprehensive investigation was made of the surface damage process. The gasdynamic parameters of the plasma flare produced in the case of surface damage were measured. The thresholds of the surface damage were measured for K-8 glass and for fused quartz.

LITERATURE CITED

1. J. F. Ready, Effects of High Power Radiation, Academic Press (1971).
2. R. W. Hopper and D. R. Uhlmann, J. Appl. Phys., 41, 4023 (1970).
3. H. S. Bennet, NBS Spec. Publ., 51, 341 (1970).
4. A. J. Glass and A. H. Guenther, Appl. Opt., 12, 637 (1973).
5. N. Bloembergen, Appl. Opt., 12, 661 (1973).
6. S. I. Anisimov and V. I. Makshantsev, Fiz. Tverd. Tela, 15, 1090 (1973).
7. V. I. Makshantsev, P. S. Kondratenko, and G. M. Gandel'man, Fiz. Tverd. Tela, 16, 173 (1974).

8. T. P. Belikova and É. A. Sviridenkov, Pis'ma Zh. Eksp. Teor. Fiz., 1, 37 (1965); 3, 394 (1966).
9. G. M. Zverev, T. N. Mikhailova, V. P. Palikov, and N. M. Solov'eva, Zh. Eksp. Teor. Fiz., 53, 184 (1967).
10. T. P. Belikova, A. N. Savchenko, and É. A. Sviridenkov, Zh. Eksp. Teor. Fiz., 54, 37 (1968); 58, 1899 (1970).
11. M. Bass and H. H. Barett, IEEE J. Quantum Electron., QE-8, No. 3, 38 (1972).
12. E. Jablonovitch, Appl. Phys. Lett., 19, 495 (1971).
13. D. W. Fradin, M. Bass, Appl. Phys. Lett., 22, 206 (1973).
14. D. W. Fradin, E. Jablonovitch, and M. Mass, Appl. Opt., 12, 700 (1973).
15. A. G. Molchanov, Fiz. Tverd. Tela, 12, 954 (1970).
16. R. A. Vlasov, K. P. Grigor'ev, I. I. Kantorovich, and G. S. Romanov, Fiz. Tverd. Tela, 15, 444 (1973).
17. A. I. Rubinshtein and V. M. Fain, Fiz. Tverd. Tela, 15, 470 (1973).
18. P. M. Mednis and V. M. Fain, Zh. Eksp. Teor. Fiz., 62, 812 (1972).
19. L. H. Holway, J. Appl. Phys., 45, 677 (1974).
20. L. V. Keldysh, Zh. Eksp. Teor. Fiz., 37, 713 (1959).
21. N. Bloembergen, Kvantovaya Elektron., 1, 786 (1974).
22. An. V. Vinogradov, in: Abstracts, Third All-Union Conf. on Physics of Interaction of Optical Radiation with Condensed Media, Leningrad (1974), p. 71.
23. S. A. Akhmanov, A. P. Sukhorukov, and R. V. Khokhlov, Usp. Fiz. Nauk, 93, No. 1, 19 (1967).
24. Yu. P. Raizer, Zh. Eksp. Teor. Fiz., 52, No. 2, 470 (1967).
25. C. R. Ginliano, Appl. Phys. Lett., 5, 137 (1964).
26. A. M. Ritus and A. A. Manenkov, Pis'ma Zh. Eksp. Teor. Fiz., 6, 927 (1967).
27. D. A. Kramer and R. E. Honig, Appl. Phys. Lett., 13, 115 (1968).
28. V. S. Starunov and I. L. Fabelinskii, Usp. Fiz. Nauk, 98, No. 3, 441 (1969).
29. N. G. Basov, O. N. Krokhin, N. V. Morachevskii, and G. V. Sklizkov, Preprint Fiz. Inst. Akad. Nauk SSSR, No. 102 (1969).
30. N. G. Basov, O. N. Krokhin, N. V. Morachevskii, and G. V. Sklizkov, in: Abstracts, First All-Union Conf. on Physics of the Action of Optical Radiation on Condensed Media, Leningrad (1969), p. 40.
31. N. G. Basov, O. N. Krokhin, N. V. Morachevskii, and G. V. Sklizkov, Zh. Prikl. Mekh. Tekh. Fiz., No. 6, 44 (1971).
32. R. G. Tomlinson, E. K. Damon, and H. T. Buscher, in: Physics of Quantum Electronics, McGraw-Hill, New York (1965), p. 520.
33. Yu. V. Afanas'ev, N. G. Basov, O. N. Krokhin, et al., Preprint Fiz. Inst. Akad. Nauk SSSR, No. 95 (1968).
34. V. A. Gribkov, A. I. Isakov, N. V. Kalachev, et al., Kvantovaya Elektron., 1, No. 2, 365 (1974).
35. B. A. Boley and J. H. Weiner, Theory of Thermal Stresses, Wiley, New York (1960).
36. G. W. C. Kaye and T. H. Laby, Tables of Physical and Chemical Constants and Some Mathematical Functions, Longmans, London (1959).
37. S. N. Zhurkov, Zh. Eksp. Teor. Fiz., 1, 189 (1931).
38. A. P. Aleksandrov and S. N. Zhurkov, The Phenomenon of Brittle Heating [in Russian], GTTI, Moscow–Leningrad (1933).
39. S. N. Zhurkov, Zh. Eksp. Teor. Fiz., 4, 161 (1934).
40. V. N. Pukh, Strength and Disintegration of Glass [in Russian], Nauka, Leningrad (1973).
41. Yu. V. Arkhipov, N. V. Morachevskii, V. V. Morozov, and F. S. Faizullov, Fiz. Tverd. Tela, 14, No. 6, 1756 (1972).
42. Yu. V. Arkhipov, N. V. Morachevskii, V. V. Morozov, and F. S. Faizullov, in: Abstracts, Second All-Union Conf. on Physics of Action of Optical Radiation on Condensed Media, Leningrad (1972), p. 5.
43. V. P. Rvachev and M. F. Sakhnovskii, Opt. Spektrosk., 18, 48 (1965).
44. Yu. V. Arkhipov, N. V. Morachevskii, V. V. Morozov, and F. S. Faizullov, Fiz. Tverd. Tela, 16, No. 1, 71 (1974).
45. N. V. Morachevskii, V. V. Morozov, and F. S. Faizullov, Preprint Fiz. Inst. Akad. Nauk SSSR, No. 40 (1975).
46. V. M. Finkel', Physics of Damage [Russian translation], Metallurgiya, Moscow (1970).
47. Yu. V. Arkhipov, N. V. Morachevskii, V. V. Morozov, and F. S. Faizullov, in: Abstracts, Third All-Union Conf. on Physics of Interaction of Optical Radiation with Condensed Media, Leningrad (1970), p. 50.

48. Yu. V. Afanas'ev and O. N. Krokhin, Zh. Eksp. Teor. Fiz., 52, 966 (1967).
49. Yu. V. Afanas'ev, N. G. Basov, O. N. Krokhin, N. V. Morachevskii, and G. V. Sklizkov, Zh. Tekh. Fiz., 39, No. 4, 894 (1969).
50. G. G. Vilenskaya and I. V. Nemchinov, Dokl. Akad. Nauk SSSR, 186, 1049 (1969).
51. I. V. Nemchinov and S. P. Popov, Zh. Prikl. Mekh. Tekh. Fiz., No. 5, 35 (1971).
52. L. D. Landau and E. M. Lifshitz, Fluid Mechanics, Pergamon (1958).
53. R. R. Teachont and R. T. Pack, Atom. Data, 3, No. 2, 195 (1971).